Observation of a single laser-excited center at the point of a crystalline needle

S. K. Sekatskiĭ[a)] and V. S. Letokhov

Institute of Spectoscopy, Russian Academy of Sciences, 142092 Troitsk, Moscow District, Russia

(Submitted 18 February 1997)
Pis'ma Zh. Éksp. Teor. Fiz. **65**, No. 6, 441–444 (25 March 1997)

The points of lithium fluoride needles are investigated by laser photoelectronic projection microscopy. A situation in which a single atomic-size source of electrons — an F_2 color center — is observed in the region near the point is realized. As a result of the good fluorescence properties of these centers, these needles can be used as the active element of a scanning fluorescence microscope employing resonance transfer of electronic excitation energy. © *1997 American Institute of Physics.* [S0021-3640(97)00106-0]

PACS numbers: 33.50.Dq, 33.60.−q

Fluorescence spectroscopy methods employing dipole–dipole resonance transfer of electronic excitation energy (fluorescence resonance energy transfer (FRET)) are now widely used for analyzing the structure and relative arrangement of complicated, primarily biological, objects (see, for example, Refs. 1 and 2 and the literature cited therein). Recently, we proposed using the phenomenon of resonance transfer of electronic excitation energy from single-atom fluorescence centers to produce a new scanning fluorescence microscope with nanometer spatial resolution and high sensitivity.[3,4] This requires a sharp microscope tip (active element) with single fluorescence centers in the aperture region. Scanning must be performed at a distance less than the characteristic range r_0 of dipole–dipole electronic excitation energy transfer from the experimental sample and the fluorescence of the sample must be recorded, in the standard manner, in the far zone. In the typical case r_0 ranges from a fraction of a nanometer to several nanometers, and since the method for scanning a tip at such distances from the sample has now been well developed in the practice of scanning tunneling and atomic-force microscopy, the most important ingredient for realizing the proposed FRET microscope is to produce sharp tips with single fluorescence centers in the region of the point.

This letter reports the observation of a single F_2 color center near the point of a LiF needle. Since the quantum yield of fluorescence of F_2 color centers in LiF crystals at room temperature is close to 1 (maximum at wavelength 670 nm, half-width 2250 cm^{-1}, cross section at maximum $7\cdot 10^{-17}$ cm^2 (Ref. 5)), the results presented can be regarded as a first realization of the active elements of a FRET microscope.

The points of the LiF needles were investigated by laser photoelectron projection microscopy, which, as was shown previously, makes it possible to visualize laser-radiation absorbing centers located close to the surface.[6,7] The idea of the method is

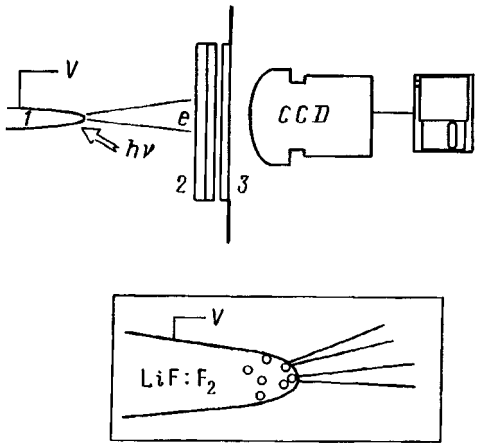

FIG. 1. Idea of the method of laser photoelectronic projection microscopy: *1* — Pointed fragment of a LiF:F_2 crystal containing color centers which absorb laser radiation $h\nu$; *2* — microchannel plate; *3* — fluorescence screen. Inset: Enlarged image of a LiF:F_2 needle point and illustration of the process of obtaining photoelectronic images of single F_2 color centers.

illustrated in Fig. 1. Sharp needles, whose points have a radius of curvature $r \simeq 0.6-1$ μm, were prepared from fragments of LiF:F_2 crystals grown at the Institute of General Physics of the Russian Academy of Sciences, by etching in concentrated hydrochloric acid. The needles prepared were employed as cathodes in a laser photoelectron projection microscope: A voltage $U=0-4$ kV was applied to the needle, and photoelectronic images of the point, which were produced by electrons emitted when a point was irradiated by radiation from a cw argon laser, were recorded. A microchannel plate– fluorescent screen assembly was used as a detector. An optical image was obtained at the output of the assembly with a TV camera and analyzed with a specialized Argus-50 processor manufactured by Hamamatsu Photonics K. K. (Japan).

The distance $L=10$ cm from the needle point to the detector determined the magnification of the microscope $M=L/\chi r$, which was equal to $3\cdot 10^4-10^5$ (here χ is a numerical coefficient, equal to 1.5–2 (see, for example, Refs. 8)). The spatial resolution of the microscope was limited by the presence of a transverse translational kinetic energy $E_\perp$ of the emitted photoelectrons and was equal to[8]

$$d \simeq 2r\chi\sqrt{E_\perp/eU}, \tag{1}$$

which for $E_\perp \sim 1$ eV gives $d \simeq 40$ nm. Additional information about the construction of the photoelectronic microscope and sample preparation as well as detailed arguments supporting the interpretation of the observed photocurrent as selective laser photoionization of F_2 color centers can be found in Ref. 7 and is not presented here. We note only that the crystalline LiF matrix itself is transparent to the laser radiation employed, while the F_2 color centers effectively absorb light in this spectral region; selective laser photoionization of these color centers has been observed before, and the basic mechanisms of this process were investigated in Ref. 9.

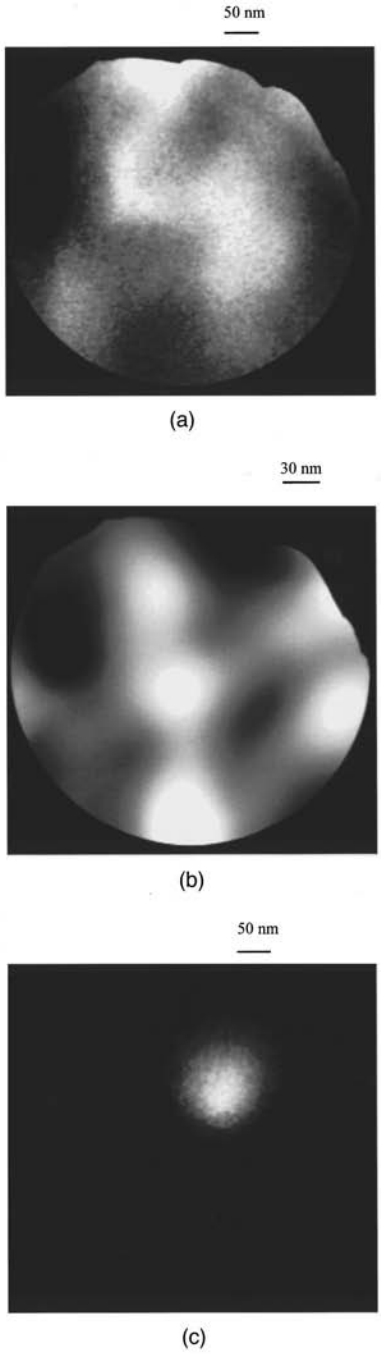

FIG. 2. Photoelectronic images of LiF:F_2 needle points. The images were obtained by irradiating the points with cw argon laser radiation with intensity $\simeq 10^4$ W/cm^2: a — Radius of curvature of the needle point $r \simeq 0.6$ μm, F_2 center density $n \simeq 10^{16}$ cm^{-3}; b — $r \simeq 1$ μm, $n \simeq 10^{16}$ cm^{-3} ; c — $r \simeq 1$ μm, $n \simeq (1\text{–}4) \cdot 10^{15}$ cm^{-3}.

Photoelectronic images of the points of different LiF:F_2 needles are displayed in Fig. 2. The needles differ from one another in respect to both the radii of curvature of the points (and therefore the magnification factor of the microscope as well) and the density n of F_2 color centers. The large uncertainty in the value of n in Fig. 2 is due to the fact that the initial samples of LiF:F_2 crystals, with a nominal F_2 color center density $\simeq 2\cdot 10^{15}$ cm^{-3}, were colored very nonuniformly, and the density of F_2 centers in the point depended on the specific part of the initial crystal from which the needle was prepared.

If the escape depth $l_{\rm esc}$ of the photoelectrons from lithium fluoride crystals is taken to be 3–10 nm, as follows from the published data,[10–12] then the observed distances l_0 between individual bright spots in Fig. 2a and 2b agree well with the estimate

$$l_0 \simeq (n l_{\rm esc})^{-1/2}. \tag{2}$$

Indeed, for $n = 10^{16}$ cm^{-3} formula (2) gives $l_0 \simeq 100-170$ nm, i.e., individual color centers should be easily resolved for needles with radii of curvature ~ 0.6 μm (Fig. 2b) and should be close to resolution for needles with $r \simeq 1$ μm (Fig. 2a). The irregularity of the arrangement of the F_2 centers in the figures reflects the random character of the production of defects in radiation-colored LiF crystals.

As the density of F_2 centers decreases further, a situation where the quantity l_0 is close to the radius of curvature r of a point and a single color center is present near the point can be realized in the sample; this is shown in Fig. 2c. For several other points prepared from the same initial LiF:F_2 crystal with average F_2 center density $n \simeq 2\cdot 10^{15}$ cm^{-3}, not one emission center could be seen in the photoelectronic images. This and the data obtained for other LiF needles with a high density of F_2 centers are consistent with the completely expected circumstance that for small average expected number $\langle n \rangle$ of color centers in the field of view of the microscope (of the order of 1–5), the number of color centers actually observed for a specific sample should undergo large fluctuations and vary strongly for different needles prepared from initial fragments with nominally the same defect density.

In summary, the results presented above attest to the fact that sharp LiF:F_2 needles with only one color center present near their points have been prepared in practice. These needles can be used as active elements in scanning fluorescence microscopes employing the phenomenon of dipole–dipole resonance transfer of electronic excitation energy. These same needles are also of interest as a source of electrons for electron holography (see, for example, Ref. 13), since they are bright atomic-size laser-induced sources of electrons.

We thank V. N. Konopskiĭ for assisting in the experiments, T. T. Basiev for preparing the LiF:F_2 crystal samples, and the company Hamamatsu Photonics K. K. for providing the experimental equipment. This work was supported in part by the Russian Fund for Fundamental Research and the US Department of Defense.

[a)]e-mail: sekats@lls.isan.troitsk.ru

[1] C. Gohlke, A. I. H. Murchie, D. M. J. Lilley, and R. M. Clegg, Proc. Natl. Acad. Sci. USA **91**, 11660 (1994).
[2] E. A. Jares-Erijman and T. M. Jovin, J. Mol. Biol. **257**, 597 (1996).
[3] S. K. Sekatskiĭ and V. S. Letokhov, JETP Lett. **63**, 319 (1996).
[4] S. K. Sekatskii and V. S. Letokhov, Appl. Phys. B **63**, 525 (1996).
[5] T. T. Basiev, S. B. Mirov, and V. V. Osiko, IEEE J. Quantum Electron. **QE-24**, 1052 (1988).
[6] V. N. Konopskiĭ, S. K. Sekatskiĭ, and V. S. Letokhov, JETP Lett. **60**, 709 (1994).
[7] V. N. Konopsky, S. K. Sekatskii, and V. S. Letokhov, Appl. Surf. Sci. **94/95**, 148 (1996).
[8] R. Gomer, *Field Emission and Field Ionization*, Harvard University Press, Cambridge, Mass., 1961.
[9] V. S. Letokhov and S. K. Sekatskiĭ, Opt. Spektrosk. **76**, 303 (1994).
[10] A. V. Aleksandrov, E. D. Aluker, I. A. Vasil'ev *et al.*, *Introduction to Radiation Physics and Chemistry of Alkali-Halide Crystal Surfaces* [in Russian], Zinatne, Riga, 1989.
[11] A. A. Maĭste, A. M. E. Saar, B. A. Sarkin, and M. A. Élango, Opt. Spektrosk. **38**, 738 (1975) [Opt. Spectrosc. (USSR) **38**, 419 (1975)].
[12] B. Quirim, W. Schwarz, Z. Wu *et al.*, Appl. Phys. Lett. **60**, 1831 (1992).
[13] A. Tomomura, *Electron Holography*, Springer, Berlin, 1994.

Translated by M. E. Alferieff

Mesoscopic oscillations of the magnetization near Ising impurity centers in strong magnetic fields

A. F. Popkov and A. I. Popov
State Scientific-Research Institute of Physical Problems, 103460 Moscow, Russia; Moscow Electronics Institute, 103498 Moscow, Russia

(Submitted 10 November 1996; resubmitted 30 January 1997)
Pis'ma Zh. Éksp. Teor. Fiz. **65**, No. 6, 445–448 (25 March 1997)

The frequency of orientational quantum oscillations of the magnetization near impurity-ion clusters with Ising properties in a saturated magnetic crystal is calculated. It is noted that in compounds of the type $Ho_xY_{3-x}Fe_5O_{12}$, where magnetic phase transitions are observed, additional magnetization reversal and magnetic resonance features due to mesoscopic oscillations of the magnetization can be observed at low concentrations $x<0.001$ and cryogenic temperatures in fields comparable to the intersublattice exchange interaction field. © *1997 American Institute of Physics.* [S0021-3640(97)00206-5]

PACS numbers: 75.60.Ej, 75.30.Hx, 75.30.Kz, 75.10.Hk

Weakly anisotropic magnetic ions — rare-earth ions R^{3+}, Co^{3+}, and others — in weakly anisotropic magnetic crystals produce demagnetization centers near which magnetic saturation is reached only in very strong fields. An example of a strong effect of a weak impurity on the magnetic behavior of a crystal is holmium-doped yttrium–iron garnet $Ho_xY_{3-x}Fe_5O_{12}$, in which magnetic phase transitions in magnetic fields comparable to the intersublattice exchange interaction field and a complicated magnetic resonance behavior at low temperatures are observed at very low concentrations $x\sim 0.001$.[1,2] At even lower concentrations $x<0.001$ the crystal cannot be regarded as magnetically homogeneous. We wish to call attention to the fact that at cryogenic temperatures additional magnetization reversal and magnetic resonance features, associated with mesoscopic oscillations of the magnetization in strong fields, can be observed in such materials. Localized magnetic states, both metastable and energetically degenerate, whose volume depends on the competition between the Zeeman and exchange energies $v_0\sim(A/HM)^{3/2}$, where A is the nonuniform exchange energy, H is the external magnetic field, and M is the magnetization of the crystal, are formed near impurity centers in magnetic-saturation fields. It is obvious that these magnetic inhomogeneities can manifest mesoscopic quantum properties at temperatures determined by the magnetic resonance frequency $T<T^*=\hbar\gamma H/k$, where γ is the gyromagnetic ratio and k is Boltzmann's constant. We shall perform a calculation and discuss the conditions for the formation of macroscopic quantum phenomena near a magnetic impurity with Ising properties.

We shall study a simplified model, in which an impurity cluster consists of n Ising ions occupying the same position in a crystal with a preferred axis oriented perpendicular to the magnetic field. We shall assume that the exchange interaction in the magnetic matrix surrounding the impurity clusters is much stronger than the relativistic and inter-

sublattice exchange interactions and that the state of magnetization of an Ising ion in a cluster is determined only by the sign of the projection of the exchange field produced by the iron sublattice. In this case, the following model Lagrangian can be used to describe the magnetization dynamics:[1,3]

$$L=-\int\left[\frac{M}{\gamma}(1-\cos\ \theta)\phi_t-MH\ \cos\ \theta-n\mu H_E\tau\ \ln\cosh\left(\frac{\sin\ \theta\ \cos\ \phi}{\tau}\right)\delta(\mathbf{r})\right.$$

$$\left.+A((\vec{\nabla}\theta)^2+(\vec{\nabla}\phi)^2\sin^2\theta)\right]d\mathbf{r}, \tag{1}$$

where θ and ϕ are the angular coordinates of the magnetization vector, $\tau=kT/\mu H_E$ is the reduced temperature, μ is the magnetic moment of an Ising ion, and H_E is the exchange interaction field between the impurity ion and the magnetic matrix of the crystal, and the Dirac delta function $\delta(\mathbf{r})$ takes into account the locality of this interaction. The first term includes allowance for the topological character of the dynamic contribution to the action of a weakly anisotropic environment. Near an impurity cluster the static magnetization distribution satisfying the Lagrange–Euler equations has the form

$$\theta\sim\theta_0\frac{a}{r}\exp(-r/w),\quad \phi=0,\pi, \tag{2}$$

where $w=(2A/HM)^{1/2}$, a is the cutoff radius of the solution ($a<w$), and θ_0 is the tilt angle of the magnetization at the center of a cluster. The equilibrium value of the tilt angle is $\theta_0=\theta_*=n\mu H_E/HMv_0\ll 1$, where $v_0=2\pi w^3$ is the volume of the magnetic inhomogeneity. In what follows, we shall make the simplifying assumption that the structure of the inhomogeneity is self-similar in time, neglecting the spin-wave retardation and assuming that only the amplitude $\theta_0(t)$ of the solution (2) and the azimuthal angle $\phi(t)$ change dynamically with time. In this approximation the Lagrangian (1) assumes the form

$$L=-v_0\left(\frac{M}{\gamma}\frac{\theta_0^2}{2}\phi_t+E\right), \tag{3}$$

where the energy density E of the system, referred to the zero level in the limiting case $\tau=0$, equals

$$E=MH\left(\frac{\theta_0^2}{2}-\theta_0\theta_*|\cos\ \phi|+\frac{\theta_*^2}{2}\right). \tag{4}$$

The equations of motion of the system (4) have the form

$$\phi_t=\gamma H\left(\frac{\theta_*}{\theta_0}|\cos\phi|-1\right),$$

$$\theta_{0t}=\gamma H\theta_*\sin\ \phi\ \mathrm{sign}(\cos\ \phi). \tag{5}$$

The linearized equations (5) show that near the equilibrium positions, $\theta=\theta_0$, $\phi=0$, π, the frequency of the magnetization oscillations, which determines the quantization energy of the quantum oscillators about the bottom of the potential well, depends only on the

external magnetic field $\omega_H = \gamma H$. For a sufficiently high potential barrier between the equilibrium positions, $U = v_0 HM\theta_*^2/2 \gg \hbar\omega_H$, the coupled oscillators can be studied in the quasiclassical approximation and the instanton theory can be used.[4,5] In this theory the frequency of quantum tunneling between the equilibrium positions is determined by an exponential function of the Euclidean action $S_E = \int iL ds$ calculated on the instanton trajectory in imaginary time $s = it$. Since the equations of motion (5) possess a first integral $E = $ const, we find the relation $\theta_0 = \pm\theta_* \exp(\pm i\phi)$ for the zero energy level, after which we obtain the desired solution from the second equation of the system (5) after integrating over imaginary time:

$$\theta_0^2 = \theta_*^2(1 - \exp(-\omega_H|s|)). \tag{6}$$

The Euclidean action equals

$$S_E = 2i\frac{v_0 M}{\gamma}\int_0^\infty \phi_s \theta_0^2 ds = \frac{v_0 M}{\gamma}\theta_*^2 = \frac{n^2\mu^2}{v_0\gamma M}\left(\frac{H_E}{H}\right)^2. \tag{7}$$

According to the instanton theory,[4] the magnetization tunneling frequency equals

$$\Gamma = p\omega_H (S_E/\hbar)^{1/2}\exp(-S_E/\hbar), \tag{8}$$

where p is a dimensionless coefficient whose value is close to 1.

Before proceeding to estimates, we note that in the above-indicated case of weakly substituted yttrium–iron garnet there are six nonequivalent sites for rare-earth ions. This makes the picture somewhat more complicated. For example, in a field parallel to the [111] axis the interaction energy of an impurity cluster with the surrounding magnetic matrix has the form

$$E = MH_E\left[\frac{\theta^2}{2} - \frac{\theta_*}{6}\tau\sum_{n=0,\pm 1}\ln\cosh\left(\frac{\cos\theta - h - \sqrt{2}\,\sin\,\theta\,\cos\left(\phi + \frac{2}{3}\pi n\right)}{\sqrt{3}\tau}\right)\right], \tag{9}$$

where θ_* has the same meaning as before, and $h = H/H_E$. In fields comparable to the exchange field, $H \sim H_E$, metastable states arise which are responsible for jump-like changes in the magnetization—the orientational phase transitions that have been studied in detail at high substitution concentrations.[1] In weakly doped compounds, where magnetic clusters with a mesoscopic volume are formed, the metastable states will spontaneously decay because of the above-described spin tunneling. For $H = H_E$, as follows from an analysis of the energy (9), the three orientationally differing phases in which

$$\theta_0 = \frac{\sqrt{2}}{3\sqrt{3}}\theta_*, \quad \phi = j\frac{2\pi}{3}, \quad j = 1,2,3$$

become energetically degenerate in the system. In a magnetic cluster the ground state will split into three pairwise-split levels on account of the tunnel coupling of the equivalent orientational phases. The off-diagonal matrix element determining the tunnel coupling of the equivalent phase states equals, in order of magnitude, the value computed above according to Eqs. (7) and (8).

We shall now make some estimates according to these formulas, taking (as in $Ho_xY_{3-x}Fe_5O_{12}$) $H_E=125$ kOe, $\mu\sim 14\,\mu_B$, where μ_B is the Bohr magneton, $M_{\mathrm{Fe}}=150$ G, and $A=2\cdot 10^{-7}$ erg/cm. Then for $H=H_E$ we find a volume of the magnetic mesoinhomogeneity is $v_0\sim 55$ nm^3, a resonance frequency $\omega_H=2\cdot 10^{12}$ s^{-1}, and a Gamow factor of $S_E/\hbar\sim 10$ for $n=30$. For this reason, the tunneling frequency will be approximately $\Gamma\sim 10^8$ s^{-1}. At temperatures below $T_*=\hbar\omega_H/k\sim 5$ K, resonance absorption of electromagnetic power — an additional magnetic resonance — can be observed at the tunneling frequency. When the number of Ising ions in an impurity cluster drops below 10, the tunneling frequency increases by three orders of magnitude. Here, however, it is obvious that the quasiclassical approximation no longer works, and furthermore the requirements for spatial and orientational uniformity of the magnetic field increase, since the tilt angle θ_* decreases.

Let us discuss the conditions for observing the expected quantum phenomena. The magnitude of the magnetic-field disorientation must be small compared with the projection of the exchange field on the Ising axis, which is responsible for the equilibrium deviation of the magnetization in the degenerate case, i.e., $\Delta H\ll H_E\theta_*$. For the parameters chosen ($n=10$) we have $\Delta H/H\ll 0.1$, which can be satisfied for real experimental conditions. The magnetostatic interaction between clusters must also be weak, so as not to impede the appearance of mesoscopic quantum effects. For this reason, the cluster density ($n=10$) should be $(r_{\mathrm{cl}})^{-3}\ll 10^{19}$ cm^{-3}, which is determined from the condition that the magnetostatic energy of a cluster $\sim(v_0M\theta_*)^2/r_{\mathrm{cl}}^3$ in the fringing fields of its neighbors be small compared with the quantum energy splitting of the ground state, $\Delta E\sim\hbar\Gamma$. The variance in the number of impurity particles in a magnetic cluster will produce an exponential variance in the tunneling frequencies and an inhomogeneous broadening of the resonance line. For this reason, the radio-pulse echo is an effective method of resonance observation of states of macroscopic quantum coherence.

We thank the Russian Fund for Fundamental Research for support (Grants 95-02-03737-a and 97-02-16183).

[1] A. K. Zvezdin, V. M. Matveev, A. A. Mukhin, and A. I. Popov, *Rare-Earth Ions in Magnetically Ordered Crystals* [in Russian], Nauka, Moscow, 1985.
[2] R. Z. Levitin, A. I. Popov, and V. V. Snegirev, Fiz. Tverd. Tela (Leningrad) **24**, 3138 (1982) [Sov. Phys. Solid State **24**, 1777 (1982)].
[3] K. P. Belov, A. K. Zvezdin, A. M. Kadomtsev, and R. Z. Levitin, *Orientational Transitions in Rare-Earth Magnets* [in Russian], Nauka, Moscow, 1979.
[4] S. Coleman, *Aspects of Symmetry*, Cambridge University Press, 1985.
[5] A. Garg and G.-H. Kim, Phys. Rev. B **45**, 12921 (1991).

Translated by M. E. Alferieff

Magnetostriction and thermal expansion anomalies near the Curie point of the compound $La_{0.7}Sr_{0.3}MnO_3$ with the perovskite structure

L. I. Koroleva[a)] and R. V. Demin
M. V. Lomonosov Moscow State University, 119899 Moscow, Russia,

A. M. Balbashov
Moscow Power Engineering Institute, 111250 Moscow, Russia

(Submitted 11 February 1997)
Pis'ma Zh. Éksp. Teor. Fiz. **65**, No. 6, 449–453 (25 March 1997)

It is found that the bulk part ω of the magnetostriction near the Curie temperature T_c in a $La_{0.7}Sr_{0.3}MnO_3$ single crystal with the perovskite structure is negative and that the temperature dependence of $|\omega|$ has a maximum near T_c. The quantity $|\omega|$ at the maximum increases rapidly with increasing magnetic field. The thermal expansion coefficient near T_c increases with temperature much faster than linearly. The paramagnetic Curie temperature determined from the Curie–Weiss law, which the paramagnetic susceptibility of this crystal satifies, was found to be lower than T_c. These anomalies and also the near-T_c metal–insulator transition which is characteristic for this material are explained by the existence of a magnetically two-phase state consisting of a conducting ferromagnetic matrix containing antiferromagnetic insulating microregions occupying not more than 5% of the sample volume. © *1997 American Institute of Physics.* [S0021-3640(97)00306-X]

PACS numbers: 75.80.+q, 75.30.Kz, 75.40.−s, 74.72.Yg

Compounds with the perovskite structure $Re_{1-x}Me_xMnO_3$, where Re are trivalent La, Pr, Y, Nd, and other rare-earth ions or a mixture of such ions and Me are divalent Sr, Ca, and Ba ions, are being intensively studied.[1] The interest in these materials is due to the giant magnetoresistance (GMR) observed in them at room temperature at a certain doping level. At the same time, the nature of the GMR in them is not clear. Attempts have been made to attribute the GMR observed in them to double Zener exchange, polaron effects due to a strong electron–phonon interaction as a result of the Jahn–Teller effect, and charge ordering. As the calculations performed in Refs. 2 and 3 showed, however, double Zener exchange along cannot explain the observed experimental facts, for example, the large values of the resistivity ρ above the Curie temperature T_c and the jump in ρ near T_c. Moreover, it predicts a weak dependence of ρ on the doping level and dependences of ρ on the magnetic field H and temperature T below T_c which are different from the observed dependences.[2] Furthermore, double Zener exchange predicts only a metallic ferromagnetic (FM) phase at low temperatures, while in compositions with $0.1 \leqslant x \leqslant 0.16$ (Re = La) the low-temperature FM phase is a semiconductor phase. In Refs. 3 and 4 it was proposed that double Zener exchange be combined with the dynamic

Jahn–Teller effect in order to explain the anomalies in ρ and the GMR in these compounds. In this manner the authors explained the metal–semiconductor transition near T_c as a transition from a polaron-type conductivity above T_c to hopping conductivity below T_c. In Refs. 5 and 6 an attempt was made to explain the neutron diffraction data for $La_{1-x}Sr_xMnO_3$ compounds ($x=0.1$ and 0.15) in a similar manner. However, this assumption cannot explain the fact that the metal–semiconductor transition temperature and the temperature of the GMR maxima are very close to the Curie point.

This letter proposes a different mechanism to explain the characteristic features of the electrical resistance, the GMR, the magnetostriction, and the thermal expansion of these materials near T_c: the presence of a magnetically two-phase state characteristic for magnetic semiconductors.[1]

In the present work we investigated the magnetization, the paramagnetic susceptibility χ, the magnetostriction λ, and the thermal expansion $\Delta l/l$ of a $La_{0.7}Sr_{0.3}MnO_3$ single crystal at temperatures from 80 to 440 K. The single crystal was grown by the floating zone method and possessed an orthorhombic structure, space group R3c, and lattice constants $a=5.511\pm0.001$ Å and $c=13.362\pm0.002$ Å at 300 K. Measurements of the magnetization, performed with a vibrating-sample magnetometer, showed that the magnetization saturates in a field $H=2$ kOe in both the easy and hard directions of magnetization. The Curie temperature determined with the aid of the method of thermodynamic Belov–Arrot coefficients was found to be equal to 371 K, which is virtually identical to the published values.[7] The temperature dependence of the paramagnetic susceptibility, measured by a torsion method, follows the Curie–Weiss law $\chi=C/(T-\Theta)$ with paramagnetic Curie point $\Theta=364$ K.

The magnetostriction and thermal expansion were measured with strain gages with resistance 92.30 ± 0.01 Ω and tensosensitivity factor 2.26. One gage was glued to the flat surface of the sample, oriented parallel to the direction of growth of the crystal, and the other gage was glued to quartz. During the measurements the gages were arranged identically on the sample and the quartz with respect to the direction of the magnetic field. The accuracy of the measurements of $\Delta l/l$ was equal to $4\cdot10^{-6}$. Figure 1 displays isotherms of the longitudinal $\lambda_\parallel$ and transverse $\lambda_\perp$ magnetostriction for some temperatures. Isotherms of the anisotropic magnetostriction $\lambda_t=\lambda_\parallel-\lambda_\perp$ and bulk magnetostriction $\omega=\lambda_\parallel+2\lambda_\perp$ were constructed from the experimental curves $\lambda_\parallel(H)$ and $\lambda_\perp(H)$. Their temperature dependences in a 9 kOe field are displayed in Fig. 2. As one can see from Fig. 2, the anisotropic part of the magnetostriction drops continuously to 0 near T_c. The curves $\lambda_t(T)$ in fields above 2 kOe are virtually identical to the curve $\lambda_t(T)$ displayed in Fig. 2. The quite large value of λ_t at low temperatures is noteworthy: $\lambda_t\cong10^{-4}$ at 100 K. As one can see from Fig. 2, the bulk magnetostriction is positive at temperatures below 280 K, but at higher temperatures it becomes negative and its absolute magnitude passes through a maximum near T_c; as the temperature increases further, $|\omega|$ decreases rapidly, approaching zero. The dependence $\omega(T)$ near T_c in different magnetic fields is shown in the inset in Fig. 2. One can see that $|\omega|_{\max}$ approximately doubles as H increases from 3 to 9 kOe. Figure 3 displays the temperature dependence of the thermal expansion coefficient $\Delta l/l$. It is well known that for dia- and paramagnets this dependence is close to linear. As one can see from Fig. 3, starting at 320 K the thermal expansion coefficient increases with temperature much more rapidly than lin-

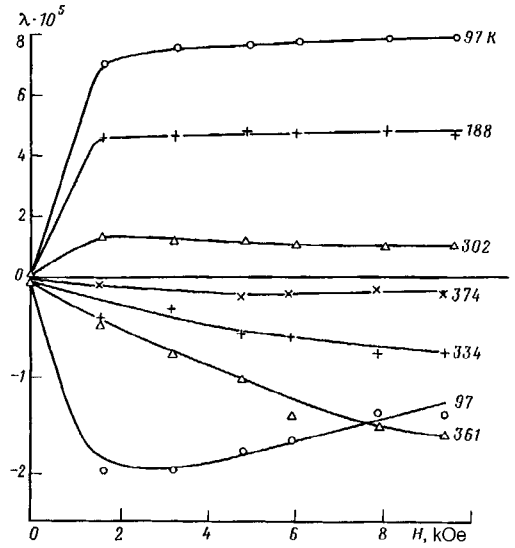

FIG. 1. Field dependence of the transverse ($\lambda<0$) and longitudinal ($\lambda>0$) magnetostriction λ at different temperatures. The temperatures (in kelvins) are indicated near the curves.

early. According to the data in Refs. 7 and 8 a metallic-type conductivity and a sharp increase in ρ near T_c were observed at the indicated composition.

A similar behavior of the magnetostriction and thermal expansion were observed in Ref. 9 in the ceramic $La_{0.6}Y_{0.07}Ca_{0.33}MnO_3$. The authors attributed the thermal expansion

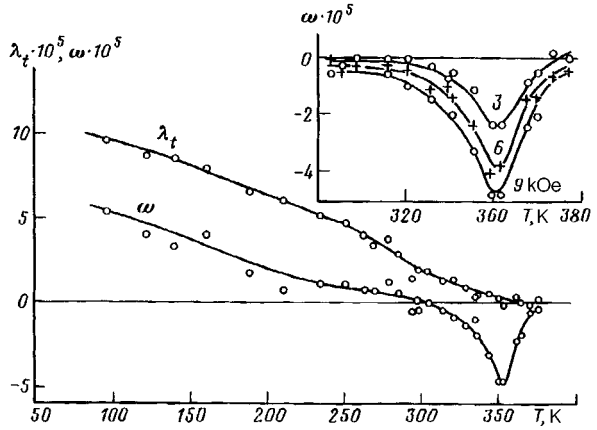

FIG. 2. Temperature dependence of the anisotropic magnetostriction λ_t and the bulk magnetostriction ω in a 9 kOe field. Inset: Temperature dependence of ω near the Curie point in different magnetic fields. The field in kOe is indicated near the curves.

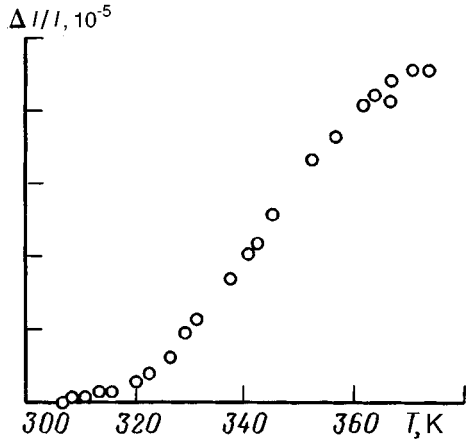

FIG. 3. Temperature dependence of the thermal expansion coefficient $\Delta l/l$.

and magnetostriction anomalies to the formation of small-radius polarons immediately above T_c. As mentioned at the beginning of this letter, this hypothesis cannot explain why polarons are formed near T_c.

The bulk magnetostriction, thermal expansion, and resistivity anomalies described above can explained by the presence of electronic separation of phases in the crystal.[1] It is well known that in magnetic semiconductors the energy of the conduction electrons is minimum at complete FM ordering in the crystal. However, the electron density in a nondegenerate antiferromagnetic (AFM) semiconductor is too low to change the state of the crystal as a whole. For this reason, on account of the gain in the *s–d* exchange energy the electrons produce in an AFM semiconductor FM microregions and stablize these regions by their self-localization in them. These microregions have been given different names by different authors who investigated them: ferrons,[1] giant quasimolecules,[10] magnetic polarons, and others. As the impurity concentration increases, such FM drops in an insulating AFM matrix increase in size, and at a sufficiently high doping level they undergo percolation. In the process, a different magnetically two-phase state is formed: Insulating AFM microregions are present in the conducting FM matrix. Yanase and Kasuya[10] showed that the lattice parameters decrease in a giant quasimolecule, since this results in screening of the new charge distribution and lowers its energy by increasing the overlapping of the charge clouds of the central ion and its closest neighbors.

The compound $La_{0.7}Sr_{0.3}MnO_3$ is a heavily doped AFM semiconductor $LaMnO_3$ in which the FM drops have coalesced, and a conducting FM phase with insulating AFM microregions has formed. This magnetically two-phase state breaks down thermally at the Curie temperature, a consequence of which is the excess thermal expansion of the sample observed in the present work (Fig. 3). However, the imposition of an external magnetic field at temperatures $T \geqslant T_c$ increases the degree of FM order near the impurities more strongly than on the average over the crystal, since the effect of the field is intensified by *s–d* exchange. That is, a magnetic field produces a magnetically two-phase state, which is destroyed by heating, and a corresponding compression of the lattice. In this manner,

the sharp increase in the negative bulk magnetostriction near T_c can be explained (Fig. 2). However, the above-indicated process of field-induced production of a magnetically two-phase state occurs in a limited temperature range not far above T_c. For this reason, the curves $|\omega|(T)$ pass through a maximum and drop rapidly as the temperature increases further.

The magnetically two-phase state is confirmed by the fact that, according to the data of Refs. 7 and 8, the spontaneous magnetization at 4.2 K for the composition studied is less than expected for complete FM ordering, specifically, it equals 95% of the latter. The fact that $T_c = 371$ K is higher than $\Theta = 364$ K attests to the presence of AFM microregions in the FM matrix. Ordinarily, $T_c \leqslant \Theta$ in FMs. It is well known that the paramagnetic Curie temperature is determined by the sum of the exchange interactions present in a crystal. The contribution of the AFM microregions to Θ decreases Θ. At the same time, the Curie temperature T_c is the magnetic transformation temperature of the simply-connected FM part of the crystal (at least when it occupies almost the entire volume of the crystal, which it does in the present case) and therefore $T_c > \Theta$.

The sharp increase in ρ near T_c is also characteristic for the above-examined magnetically two-phase state. Nagaev showed[1] that for the indicated form of the magnetically two-phase state there are two mechanisms by which the impurity-magnetic interaction influences the resistance: scattering of charge carriers, which decreases their mobility, and formation of a tail, consisting of localized states, in the carrier band. In Ref. 1 it is shown that near T_c the charge-carrier mobility decreases rapidly and the charge carriers become partially localized in the band tail.

In summary, the unusual properties of this material near T_c can be explained with the aid of a magnetically two-phase state: the sharp increase in the thermal expansion coefficient, the maximum of the absolute value of the negative bulk magnetostriction, the sharp increase in the resistivity, and the fact that $T_c > \Theta$.

This work was supported by the Russian Fund for Fundamental Research.

[a)]e-mail: koroleva@rem.phys.msu.su

[1] É. L. Nagaev, Usp. Fiz. Nauk **166,** 833 (1996).
[2] A. J. Millis, P. B. Littlewood, and B. I. Shraiman, Phys. Rev. Lett. **74**, 5144 (1995).
[3] A. J. Millis, and B. I. Shraiman, and R. Mueller, Phys. Rev. Lett. **77**, 175 (1996).
[4] A. J. Millis, Phys. Rev. B **53**, 8434 (1996).
[5] Y. Yamada, O. Hino, S. Nohdo, and R. Kanao, Phys. Rev. Lett. **77**, 904 (1996).
[6] S. J. L. Billinge, R. J. DiFrancesco, G. H. Kwei *et al.*, Phys. Rev. Lett. **77**, 715 (1996).
[7] A. Urushibara, Y. Moritomo, T. Arima *et al.*, Phys. Rev. B **51**, 14103 (1995).
[8] H. Y. Hwang, S.-W. Cheong, N. P. Ong, and B. Battlogg, Phys. Rev. Lett. **77**, 2041 (1996).
[9] M. R. Ibarra, P. A. Algarabel, C. Marquina *et al.*, Phys. Rev. Lett. **75**, 3541 (1995).
[10] A. Yanase and T. Kasuya, J. Phys. Soc. Jpn. **25**, 1025 (1968).

Translated by M. E. Alferieff

Negative ions in liquid helium: existence of new bound states

S. K. Sekatskiĭ[a)]

Institute of Spectroscopy, Russian Academy of Sciences, 142092 Troitsk, Moscow Region, Russia

(Submitted 10 December 1996; resubmitted 11 February 1997)
Pis'ma Zh. Éksp. Teor. Fiz. **65**, No. 6, 454–458 (25 March 1997)

It is shown that fundamentally new bound states can be formed when a foreign negative ion is embedded in liquid helium. For such states the excess electron forms a bubble with a radius $R_0 \simeq 17-18$ Å, and a foreign neutral atom is trapped inside this bubble because of the polarization interaction with the electric field of the excess electron, which has a maximum at a point $r \simeq R_0/2$. The main properties of such structures are considered. © *1997 American Institute of Physics.* [S0021-3640(97)00406-4]

PACS numbers: 39.90.+f, 67.55.Lf

It is well known that an excess electron embedded in liquid helium-4 pushes away the helium atoms and resides in a bubble with a radius of 17–18 Å at zero pressure.[1] This occurs because the repulsive interaction of an excess electron with helium atoms at typical interatomic distances is strong (the barrier U_0 for penetration of a free electron into liquid helium is 1.02 eV; Ref. 2) and the surface tension of helium is small. Various properties of such bubbles have now been rather well studied both experimentally and theoretically (see, e.g., Refs. 1–4 and references cited therein).

Relatively recently the spectral and other characteristics of neutral atoms and positive ions embedded in liquid helium have also become a rather popular object of study, and a number of experimental[5–7] and theoretical[8–11] investigations in the field have been carried out. It has been shown that the main properties of such atoms and positive ions are reasonably well characterized by the model of a spherical bubble-like state, analogous to the free electron case: foreign atoms and ions embedded in liquid helium create bubbles with radii $R \sim 8-13$ Å through the repulsive interaction of the helium atoms with the outer valence electron of the foreign atom or ion.

In this letter we would like to call attention to the fact that bound states of a fundamentally new type can be formed in the case of *negative* ions implanted in liquid helium. For these states a quasifree excess electron creates a bubble of radius R_0, and a foreign neutral atom is localized *inside* this bubble through the polarization interaction with the electric field of the excess electron, which has a maximum at $r \simeq R_0/2$. In this case the excess electron can be regarded as the ''nucleus'' and a neutral atom can be regarded as the ''electron'' of a new kind of atom.

The wave function $\psi(r)$ of an electron in a bubble of radius R_0 can be written as[3,12]

$$\psi(r)=\frac{A}{r}\sin(k_0 r) \quad \text{for } r\leqslant R_0, \tag{1}$$

$$\psi(r)=\frac{B}{r}\exp(-kr) \quad \text{for } r\geqslant R_0, \tag{2}$$

where

$$k=\sqrt{2U_0-k_0^2}. \tag{3}$$

(Here and below, unless specifically stated to the contrary, the system of atomic units with $m=e=\hbar=1$ will be used.) The value of k_0 can be found from the condition of matching the ratio ψ'/ψ for (1) and (2) at the point $r=R_0$:

$$\tan(k_0 R_0)=-\frac{k_0}{k}, \tag{4}$$

and A and B are normalization constants which can be found from the usual relation $\int\psi^2 r^2 dr=1$. In the case of the simplest model of an impenetrable spherical square well potential barrier at $r=R_0$ the relation (4) is replaced by the condition $\psi(R_0)=0$, which for the $1s$ ground state of the electron in a bubble gives $k_0=\pi/R_0$. For the subsequent discussion we shall use for R_0 the value obtained from the experimental data of Grimes and Adams,[4] who found for the case of zero external pressure that $R_0=17.2$ Å $=32.5$ atomic units. Using this value and the barrier height $U_0=1.02$ eV$=0.0375$, one easily finds that $k_0=0.084$, $k=0.26$, and $A=0.231$, and thus for $r\leqslant R_0$ one has

$$\psi(r)=\frac{0.231}{r}\sin(0.084r). \tag{5}$$

Let us define $q(r)$ as the total electric charge contained in the region $0\leqslant r_1\leqslant r$ $(r\leqslant R_0)$; then

$$q(r)=\int_0^r \psi^2(r_1)r_1^2 dr_1=\frac{A^2}{2}\left(r-\frac{\sin(2k_0 r)}{2k_0}\right). \tag{6}$$

The electric field strength accociated with the charge distribution (6) is:

$$E(r)=\frac{q(r)}{r^2}=\frac{A^2}{2}\left(\frac{1}{r}-\frac{\sin(2k_0 r)}{2k_0 r^2}\right) \tag{7}$$

For the subsequent discussion the most important fact is that the electric field strength $E(r)$ (7) has a maximum at $r_0=\pi/2k_0=18.7=9.9$ Å *inside* the bubble. (For the above-mentioned simplest model of the impenetrable square-well barrier, $r_0=R_0/2=8.6$ Å.) It means that the energy of interaction between an atom with a polarizability α and the electric field E of the excess electron

$$U=-\frac{1}{2}\alpha E^2 \tag{8}$$

has a minimum at the same radius $r=r_0$, and this atom can be trapped in the vicinity of this point and form a bound system of a new type. The potential energy of this polariza-

tion interaction is fairly high, and for many atoms it is much higher than the typical thermal energy of liquid helium. For example, for a lithium atom of polarizability $\alpha=160$ (Ref. 13) this energy is $1.6\cdot 10^{-4}=51$ K, while for a magnesium atom ($\alpha=74$; Ref. 13) one has $U\simeq 24$ K, etc. (here the polarizability unit in the Coulomb system $a_0^3=1.48\cdot 10^{-25}$ cm^{-3} is used, where a_0 is the Bohr radius). At the same time, the energy of the polarization interaction is much smaller than the energy of the $1s$ ground state of an electron in the bubble, $E_0=k_0^2/2=7\cdot 10^{-3}=0.19$ eV, and thus the excess electron can indeed be treated as a quasifree one, for which this interaction represents a relatively small correction to its repulsive interaction with liquid helium. We believe that such a relation between the typical energies of interaction between an excess electron and a foreign atom and between an excess electron and liquid helium justify the use of the simple model considered in this paper. A more detailed analysis of energy states for the system considered will be published later elsewhere. For such an analysis it is necessary to take into account some factors which have been neglected here: first of all an additional repulsive interaction of helium atoms with the outer valence electron of a foreign atom inside a bubble,[8–11] etc. At the same time, it should be noted that the maximum electric field strength in the case considered is equal to $\simeq 7\cdot 10^6$ V/cm, i.e., exactly of the same order of magnitude (even slightly below) as that available in experiments on the field evaporation of atoms adsorbed on sharp metal tips (see, e.g., Ref. 14 and references cited therein). Those experiments have revealed that the interaction between the electric field and the atom can be satisfactorily described by the simple polarization potential (8), even for such strong fields, which is an additional justification of the model used in the present work.

Note that the values of r_0 and R_0-r_0 are somewhat larger than the typical Hartree radii of light atoms, $r_{\text{at}}\sim 2-4$ Å (Ref. 13), and the effective mass of the bubble, which is ~ 240 times the mass of a ^{4}He atom[1,11] is much larger than the mass of a foreign neutral atom. Thus the system considered can indeed be regarded as a new kind of atom in which the ''light electron'' (a neutral atom) is orbiting ''in vacuum'' (inside a bubble) around a ''heavy nucleus'' (an excess electron which forms a bubble).

To estimate roughly the total number N of bound states in the system considered we can use the well-known semiclassical result of Pokrovskiĭ: for the case of a spherically-symmetric interaction potential this number can be expressed by the integral[12]

$$N\simeq \frac{M}{4}\int_0^{R_0}(-U)rdr=\frac{M\alpha A^4}{32}\int_0^{R_0}\left(\frac{1}{r}-\frac{\sin(2k_0r)}{2k_0r^2}\right)^2 rdr. \tag{9}$$

For the case of the lithium atom such an estimate gives $N\simeq 200$, and for the magnesium atom, $N\simeq 370$, which are much greater than unity (the value of the final integral in Eq. (9) is 1.10).

The energy levels $E_{n,l}$ of the system considered can be found from the usual semiclassical quantization condition:[12,15]

$$\int_{r_1}^{r_2}\sqrt{2M\left(\frac{\alpha E^2}{2}-\frac{1}{2Mr^2}(l+1/2)^2+E_{n,l}\right)}=\pi(n+1/2), \tag{10}$$

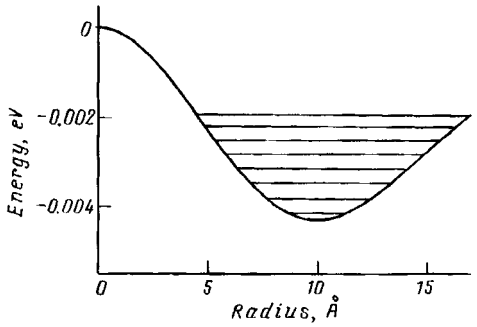

FIG. 1. An interaction potential and energy levels of the bound states of a lithium atom residing inside a bubble created by an excess electron for the case $l=0$.

where M is the mass of the foreign neutral atom, l is the angular momentum, and n is an integer designating the number of energy states with a given l value. The energy $E(r)$ can be found from relation (7), and r_1, r_2 are the roots of the equation

$$\frac{\alpha E^2}{2}+E_{n,l}-\frac{(l+1/2)^2}{2Mr^2}=0; \tag{11}$$

for angular momentum $l=0$ the term containing $(l+1/2)^2$ in (10) should be omitted. Generally such a semiclassical quantization procedure gives precise results only at large n and l values, but the results of such calculations are frequently used[12,15] for the qualitative evaluation of the energies of states with even the smallest n and l. Some of these results for the cases of lithium and magnesium atoms are shown in Fig. 1. It can be seen that the energy difference between different (n,l) and $(n,l+1)$ states with the same principal quantum number n and neighboring angular momenta l, $l+1$ is very small: this difference is of the order of $\sim 3\cdot 10^{-5}$ eV for $n=1$ and decreases rapidly with increasing n. Certainly such a small energy difference is due to the large foreign atom mass M: it is easy to see that for not very large l the first term in (10) (polarization attraction) is much larger than the second term (centripetal potential). The sequence of energy levels for the case of lithium atom is as follows: $1s$, $1p$, $1d$, ..., $1\ l=11$, $2s$, $2p$, $2d$, $1\ l=12$, $2f$, $2g$, $1\ l=13$, $2h$, $2\ l=6$, $1\ l=14$, $2\ l=7$, $2\ l=8$, $1\ l=15$, $2\ l=9$, $1\ l=16$, $2\ l=10$, $3s$, etc. Note that as in the case of a free excess electron, a number of dipole allowed radiative transitions between the considered different states of negative ions in liquid helium should exist.

Calculations based on formulas (10) or (9) show that bound states cannot exist for the atoms with very small polarizability. Neither, certainly, can such states exist for atoms for which the electron–atom repulsion dominates (such as helium or neon). In this case the ''electron pressure'' effect will be the most important: such an embedded atom, which is ''impenetrable'' to the electron, decreases the volume of the region in which the excess electron is localized, which leads to an increase in the energy of this localized electron. Thus the electron tends to push these atoms out of the bubble; quantitatively this process can be descibed using a concept of a localized electron pressure — see, e.g., Ref. 1 and references cited therein.

Thus we have shown that negative ions embedded in liquid helium can form bound states of a fundamentally new type. For atoms which can form free stable negative ions (such as lithium) these states can be regarded as a highly excited metastable states of a different nature from that of the ground state of a free negative ion. For such atoms which cannot form free stable negative ions but at the same time have non-negligible polarizability (such as magnesium) these states are the only possible bound states of the negative ion (which in this case can exist only inside liquid helium). Certainly an experimental study of such states would be very interesting from the standpoint of the physics of particles embedded in liquid helium and the physics of the excess-electron–neutral-atom interaction. It seems that such systems (even for the case of atoms which cannot form free stable negative ions) can be prepared using the same technique of laser sputtering of samples embedded in liquid helium, which has already been successfully used for neutral-atom implantation in liquid helium.[16] Analogous energy states can be realized also for negative ions trapped inside of cryodielectrics other than liquid helium with a negative electron affinity (liquid and solid hydrogen, neon, etc.).[1] The case of solid hydrogen is especially interesting because here the dimensions of the trap are not governed by the value of the surface tension and can be arbitrary.

[a)]e-mail: lls@isan.msk.su

---

[1] V. B. Shikin and Yu. P. Monarkha, *Two-Dimensional Charged Systems in Liquid Helium* [in Russian] Nauka, Moscow, 1983.
[2] M. A. Woolf and G. W. Rayfield, Phys. Rev. Lett. **15**, 235 (1965).
[3] B. E. Springett, M. H. Cohen, and J. Jortner, Phys. Rev. **159**, 183 (1967).
[4] C. C. Grimes and G. Adams, Phys. Rev. B **41**, 6366 (1990).
[5] H. Bauer, M. Beau, A. Bernhardt *et al.*, Phys. Lett. A **137**, 217 (1989).
[6] H. Bauer, M. Beau, B. Friedl *et al.*, Phys. Lett. A **146**, 134 (1990).
[7] Y. Takahasi, K. Sano, T. Kinoshita, and T. Yabuzaki, Phys. Rev. Lett. **71**, 1035 (1993).
[8] A. P. Hickman, W. Steets, and N. F. Lane, Phys. Rev. B **12**, 3705 (1975).
[9] M. W. Cole and R. A. Bachman, Phys. Rev. B **15**, 1388 (1977).
[10] C. S. Murphy and P. K. Swaminathan, J. Chem. Phys. **90**, 2776 (1989).
[11] K. E. Kurten and M. L. Ristig, Phys. Rev. B **27**, 5476 (1983).
[12] L. D. Landau and E. M. Lifshits, *Quantum Mechanics* (Pergamon Press, Oxford, 1958) [Russian original, Ogiz, Moscow-Leningrad, 1948].
[13] A. A. Radtsig and B. M. Smirnov, *Parameters of Atoms and Atomic Ions* [in Russian], Énergoatomizdat, Moscow, 1986.
[14] E. W. Müller and T. T. Tsong, *Field Ion Microscopy, Field Ionization and Field Evaporation* (Pergamon Press, Oxford 1973).
[15] D. J. Simms and N. M. J. Woodhouse, *Lectures on Geometric Quantization* (Springer-Verlag, Berlin, 1976).
[16] A. Fujisaki, K. Sano, T. Kinoshita *et al.*, Phys. Rev. Lett. **71**, 1039 (1993).

Published in English in the original Russian journal. Edited by James Anderson and Steve Torstveit.

Competition between single- and multiparticle resonances in tunneling

K. A. Kikoin and L. A. Manakova
Kurchatov Institute Russian Science Center, 123182 Moscow, Russia

(Submitted 13 February 1997)
Pis'ma Zh. Éksp. Teor. Fiz. **65**, No. 6, 459–464 (25 March 1997)

A new mechanism is proposed for the anomalous tunneling transmittance of a double-barrier quantum-well structure doped with a transition-metal impurity and possessing an intrinsic two-dimensional continuum. The new tunneling channels are due to exponentially-narrow single-particle resonances arising near the edge of a 2D band during tunneling. They are temperature-independent and their contribution to the transmittance can exceed the contribution of the Kondo resonance even at temperatures $T<T_K$. © *1997 American Institute of Physics.* [S0021-3640(97)00506-9]

PACS numbers: 73.40.Gk, 73.20.Dx, 72.15.Eb, 71.20.Be

1. A resonance increase in the tunneling transmittance is observed in different quantum structures with negative differential resistance (see references cited in Ref. 1). These structures often possess the energy profile of a double-barrier quantum well (DBQW) with metallic walls. Until now tunneling through a DBQW has been regarded as tunneling through a localized state,[2] since the role of the 2D continuum was assumed to be trivial. Naturally, the mechanisms of tunneling through a quantum well and tunneling through a resonance level under a barrier were not distinguished.[3] The increase in the tunneling transmittance was attributed to multiparticle effects: Kondo scattering with strong Coulomb repulsion on a localized level[4] and Coulomb interaction between metallic carriers in the walls and an electron on a localized level.[5] As is well known,[6] these multiparticle peaks are very sensitive to the temperature and magnetic field.

This letter proposes a new mechanism of resonance tunneling that can be observed in GaAlAs/GaAs/GaAlAs structures doped with transition-metal impurities. New tunneling channels appear because the internal GaAs layer has an intrinsic two-dimensional continuum of spatially quantized band states. In the process of tunneling through a quantum well doped with a $3d$ impurity, new exponentially narrow resonance states with widths much less than the tunneling widths form near the edges of the 2D bands. As a result, strong resonance tunneling becomes possible when the Fermi level of the walls is not in resonance with quasilocalized (deep) impurity levels. An exponential increase in the transmittance (in an elementary tunneling event) in new channels is possible even before the interactions are considered. When the Kondo scattering of electrons from the Fermi level in the walls by an impurity level in a well is taken into account, the result obtained below is that even at temperatures $T<T_K$ the new edge resonances arising in the process of tunneling, and not the Kondo resonance, can make the main contribution to the transmittance. It is important that the new resonances do not depend on the temperature

and persist for $T \gg T_K$, where the Kondo resonance vanishes completely.

2. We are studying a situation when a transition-metal impurity engenders a deep level with energy E_{id} in the band gap of the GaAs layer. This layer also possesses a two-dimensional continuum with a dispersion law $\epsilon_{\mathbf{k}_\perp}$. We shall study the case when the Fermi level in the boundaries lies near the bottom of the conduction band of the interior layer. The Hamiltonian of the system has the form $H = H_0 + H_t$, where

$$H_0 = \sum_{\mathbf{k},\nu=L,R} \epsilon^\nu_{\mathbf{k}} a^+_{\mathbf{k}\sigma\nu} a_{\mathbf{k}\sigma\nu} + \sum_\sigma \left(E_{id} d^+_\sigma d_\sigma + \frac{U}{2} n_{d\sigma} n_{d-\sigma} \right) + \sum_{\mathbf{k}} \varepsilon_{\mathbf{k}_\perp} c^+_{\mathbf{k}_\perp} c_{\mathbf{k}_\perp}, \tag{1}$$

$$H_t = H_{td} + H_{tc} = \sum_{\mathbf{k}\nu\sigma} (T^\nu_{\mathbf{k}d} a^+_{\mathbf{k}\nu\sigma} d_\sigma + \text{h.c.}) + \sum_{\mathbf{k}\nu\sigma} \sum_{\mathbf{k}_\perp'} (T^\nu_{\mathbf{k}\mathbf{k}'} a^+_{\mathbf{k}\nu\sigma} c_{\mathbf{k}_\perp'} + \text{h.c.}). \tag{2}$$

The operators $a_{\mathbf{k}_{\nu\sigma}}$ describe the electronic states in the left-hand (L) and right-hand (R) boundaries of the tunneling contact. The operators d_σ and $c_{\mathbf{k}_\perp}$ of the localized and itinerant states in a well correspond to the wave functions[7]

$$\psi_{id}(\mathbf{r}) = A_d^{-1/2} \left[\varphi_d(\mathbf{r}) + \sum_{\mathbf{k}_\perp} B(\mathbf{k}_\perp) \phi(\mathbf{k}_\perp, \mathbf{r}) \right],$$

and

$$\psi_{\mathbf{k}_\perp}(\mathbf{r}) = A_0^{-1/2} \left[\phi_{\mathbf{k}_\perp}(\mathbf{r}) - A_d^{-1/2} \left(\sum_{\mathbf{k}'_\perp} A_{\mathbf{k}_\perp \mathbf{k}'_\perp} \phi_{\mathbf{k}'_\perp}(\mathbf{r}) + B(\mathbf{k}_\perp) \varphi_d(\mathbf{r}) \right) \right].$$

Here $B(\mathbf{k}_\perp) = V^d_{\mathbf{k}_\perp} / (E_{id} - \varepsilon_{\mathbf{k}_\perp})$; $A_{\mathbf{k}_\perp \mathbf{k}'_\perp} = \tilde{A}_d B(\mathbf{k}_\perp) B(\mathbf{k}'_\perp)$; $\tilde{A}_d$, A_d, and A_0 are normalization factors; and, $V^d_{\mathbf{k}_\perp} \approx V_d$ is the hybridization matrix element in a well. With the aid of these wave functions it is easy to find the tunneling matrix elements in Eq. (2):

$$T^\nu_{\mathbf{k}d} = B(\mathbf{k}_\perp) T^\nu_d(k_l), \quad T^\nu_{\mathbf{k},\mathbf{k}'_\perp} = (T^\nu_0(k_l) \delta_{\mathbf{k}_\perp \mathbf{k}'_\perp} + T^\nu_c(k_l) B(\mathbf{k}_\perp) B(\mathbf{k}'_\perp)). \tag{3}$$

Here $\mathbf{k} = \mathbf{k}_\perp$, k_l and it was assumed that the longitudinal and transverse motions of the electrons in the walls are separated: $\varepsilon_{\mathbf{k}} = \varepsilon_{\mathbf{k}_\perp} + \varepsilon_{k_l}$. The matrix elements $T^\nu_0(k_l)$, $T^\nu_d(k_l)$, and $T^\nu_c(k_l)$ differ from one another by factors consisting of the normalization constants, but all three quantities are proportional to the matrix element of the tunneling potential between the longitudinal components of the wave functions in the walls ν and in the defect layer: $T_\nu(k_l) = \int \psi^*_\nu(k_l, z) V(z) \phi(k_l, z) dz$. In contrast to the standard tunneling problem, in our case there is no direct overlapping between the atomic impurity wave function $\varphi_d(\mathbf{r})$ and the itinerant states in the walls. The only source of tunneling is the overlapping between the Bloch states of the defect layer and the walls. The tunneling Hamiltonian contains, besides the standard term H_{td} (which exists, however, only on account of the presence of the ''Bloch tail'' in the impurity wave function), a second term H_{tc}. This is the term giving rise to the new resonance states near the edge of the 2D band.

Before proceeding to the solution of the impurity tunneling problem, we shall examine the rearrangement of the band spectrum in the well on account of tunneling

between the walls and the well. This tunneling is described by the term with $T_0^{\nu}(k_l)$ in $T^{\nu}_{\mathbf{k},\mathbf{k}'_{\perp}}$. The renormalized spectrum $\widetilde{\varepsilon}_{\mathbf{k}_{\perp}}$ is determined by the equation

$$\widetilde{\varepsilon}_{\mathbf{k}_{\perp}} = \varepsilon_{\mathbf{k}_{\perp}} + \sum_{k_l,\nu} \frac{|T_0^{\nu}(k_l)|^2}{\widetilde{\varepsilon}_{\mathbf{k}_{\perp}} - \varepsilon^{\nu}_{\mathbf{k}_{\perp}} - \varepsilon^{\nu}_{k_l}}. \tag{4}$$

It follows from the solution of this equation that ''*evanescent*'' states with complex wave vectors $\mathbf{k}_{\perp}$ and complex energies $\widetilde{\varepsilon}_{\mathbf{k}_{\perp}}$ such that Re $\mathbf{k}_{\perp} \approx$ Im $\mathbf{k}_{\perp}$ form near the bottom of the 2D band. These states exist in the region $\varepsilon - \varepsilon_c < \gamma_0 \ll W$ and are described by the density of states

$$\rho_c(\varepsilon) = \frac{\rho_{0c}}{\pi}\left[\arctan\frac{\varepsilon-\varepsilon_c}{\gamma_0} - \arctan\frac{\varepsilon - W}{\gamma_0}\right] \tag{5}$$

(ρ_{0c} is the threshold density of states of the unperturbed 2D band; ε_c and W are the edge and width of the 2D band, respectively; γ_0 is the imaginary part of the self-energy in Eq. (4) with $\widetilde{\varepsilon}_{\mathbf{k}_{\perp}} = \varepsilon_c$; and, we neglect the weak shift of the band energies in Eq. (5)). We underscore that the evanescent states exist because tunneling occurs between bands of different dimension (3D band in the wall and 2D band in the well).

Therefore only the impurity term, which is proportional to $T_c^{\nu}(k_l)$ in Eq. (3), remains in the tunneling Hamiltonian H_{tc} in the important range of energies, but the density of states of the 2D continuum is determined by expression (5).

3. Another source of characteristic features generated by a d impurity is the Hubbard repulsion **U** between electrons in a deep level. Strong Coulomb repulsion in our case can engender only an indirect interaction between electrons in the walls and at a d level. This interaction is due to the overlapping of the itinerant states of the walls and the ''Bloch tail'' of the impurity wave function. To derive this interaction we employ the fact that the first two terms in the Hamiltonian H_0 together with the term H_{td} in the tunneling Hamiltonian form an Anderson model Hamiltonian. It is convenient to solve this standard problem first in the limit of large U by one of the methods developed for the Kondo problem,[8] and then to use this solution as a basis for the tunneling problem. Since $|T_d^{\nu}|^2 \rho_{\nu} E_{id} \ll 1$ for a deep level (ρ_{ν} is the density of states in the boundaries), then by means of the Schrieffer–Wolf transformation we obtain from the Hamiltonian $H_0 + H_{td}$ the effective Hamiltonian $H_{\text{eff}} = \widetilde{H}_0 + H_{ex}$, where $\widetilde{H}_0$ is the Hamiltonian (1) without the Coulomb term and H_{ex} is the exchange interaction between electrons at the Fermi level in the walls and a d electron. When the Kondo scattering is taken into account, the Green's function $\mathcal{G}_{d\sigma}(z)$ of quasilocalized electrons and the $\mathcal{T}$ matrix for electrons in the side plates can be calculated by the equation of motion method.[8,9] They are determined by the expressions

$$\mathcal{T}^{\nu\nu}_{d\sigma}(z,\mathbf{k}\mathbf{k}') = T^{\nu *}_{\mathbf{k}d}\mathcal{G}_{d\sigma}(z)T^{\nu}_{\mathbf{k}'d}, \quad \mathcal{G}_{d\sigma}(z) = \frac{1}{z - \epsilon_{d\sigma} - i\gamma_d - \Sigma_K(z)},$$

$$\epsilon_{d\sigma} - i\gamma_d = \sum_{\mathbf{k},\nu} \frac{|T^{\nu}_{\mathbf{k}d}|^2}{z - \epsilon^{\nu}_{\mathbf{k}}}.$$

For $|z|$ close to the Fermi level we obtain

$$\Sigma_K(z)=\sum_{\mathbf{k},\nu}\frac{|T^{\nu}_{\mathbf{k}d}|^2 f(\epsilon^{\nu}_{\mathbf{k}})}{z-\epsilon^{\nu}_{\mathbf{k}}}\sim\gamma_d\ \mathrm{Ln}\ \frac{W_\nu}{z-\mu},\quad \mathcal{G}_{d\sigma}\approx\frac{\mathcal{Z}_K}{z-E_K}. \tag{6}$$

Here $E_K=\mu+i\gamma_K$, γ_K is of the order of the Kondo temperature $T_K\sim(W_\nu\gamma_d)^{1/2}\mathcal{Z}_K$, and W_ν is the width of the band in the side plates.

So, taking account of Kondo scattering the tunneling problem is described by the Hamiltonian $H=H_{\mathrm{eff}}+\tilde{H}_{tc}$, where $\tilde{H}_{tc}$ is the tunneling Hamiltonian with matrix elements which are renormalized with partial diagonalization of H. We call attention to the fact that without the interaction the Hamiltonian H in Eqs. (1) and (2) describes our tunneling problem exactly. At the same time, in the absence of a 2D continuum in the well and thereby the term H_{tc}, the well-known Glazman–Raĭkh solution is obtained for the tunneling problem.[4] The ''switching on'' of the tunneling term H_{tc} results in additional potential scattering inside the quantum well, which reproduces exponentially narrow single-particle resonances near the edge of the 2D band in the well. The scattering matrix of an electron inside the well is determined from the Green's function

$$\mathcal{G}^{cc}_{\sigma}(\mathbf{k}_\perp,\mathbf{k}'_\perp;z)=\langle c_{\mathbf{k}_\perp}|\hat{I}(z-\hat{H})^{-1}|c_{\mathbf{k}'_\perp}\rangle=\delta_{\mathbf{k}_\perp,\mathbf{k}'_\perp}\mathcal{G}_{0\mathbf{k}_\perp}(z)$$
$$+\mathcal{G}_{0\mathbf{k}_\perp}(z)\mathcal{T}^{cc}_{\sigma}(\mathbf{k}_\perp,\mathbf{k}'_\perp;z)\mathcal{G}_{0\mathbf{k}'_\perp}(z).$$

Here $\hat{I}$ is a unit matrix, $\mathcal{G}_{0\mathbf{k}_\perp}(z)=[z-\tilde{\varepsilon}_{\mathbf{k}_\perp}]^{-1}$,

$$\mathcal{T}^{cc}_{\sigma}(\mathbf{k}_\perp,\mathbf{k}'_\perp;z)=\frac{T_0(z)}{1-T_0(z)J_c(z)}B(\mathbf{k}_\perp)B^*(\mathbf{k}'_\perp),\quad T_0(z)=|\Sigma_{dc}(z)|^2\mathcal{G}_{d\sigma}(z)+\Sigma_{cc}(z), \tag{7}$$

$$\Sigma_{cc}(z)=\sum_{\mathbf{k},\nu}\frac{|T^{\nu}_{\mathbf{k}c}|^2}{z-\varepsilon^{\nu}_{\mathbf{k}}},\quad \Sigma_{dc}(z)=\sum_{\mathbf{k},\nu}\frac{T^{\nu *}_{\mathbf{k}c}T^{\nu}_{\mathbf{k}d}}{z-\varepsilon^{\nu}_{\mathbf{k}}},\quad J_c(z)=\sum_{\mathbf{k}_\perp}\frac{|B_s(\mathbf{k}_\perp)|^2}{z-\tilde{\varepsilon}_{\mathbf{k}_\perp}}.$$

The functions $\Sigma_{cc}(z)$ and $\Sigma_{dc}(z)$ are the Hilbert transforms of the three-dimensional density of states of the side plates ''weighted'' with the tunneling integrals. In the important region of the spectrum near the band edge these are smooth functions of the energy as compared with $J_c(z)$. The integral $J_c(z)$ is the Hilbert transform of the quasi-two-dimensional density of states $\rho_c(\varepsilon)$ defined in Eq. (5). For $|z-\varepsilon_c|/\gamma_0\ll 1$ this integral has a logarithmic singularity

$$J_c(z)=\int d\varepsilon\frac{\rho_c(\varepsilon)|B_s(\varepsilon)|^2}{z-\varepsilon}=-\frac{1}{2}\tilde{\rho}_{0c}\ \mathrm{Ln}\left(\frac{z-\varepsilon_c}{\gamma_0}\right),\quad \tilde{\rho}_{0c}=\rho_{0c}(\varepsilon_c)|B_s(\varepsilon_c)|^2. \tag{8}$$

The Green's function $\mathcal{G}^{cc}_{\mathbf{k}_\perp,\mathbf{k}'_\perp}(z)$ determines completely the probability of elastic tunneling through the quantum well (see below). We shall not study the standard contribution to the tunneling amplitude engendered by the impurity level $E_d=\epsilon_{d\sigma}-i\gamma_d$; this contribution has been studied in many works. We wish to call attention below to the additional features which appear in the spectrum of a quantum well as a result of tunnel-

ing transitions between the well and the side plates. The self-consistent equation $1-T_0(z)J_c(z)=0$ on the low-energy poles of the scattering matrix $\mathcal{T}^{cc}(z)$ has in our case the form

$$z-E_K-[\Sigma_{cc}(z)(z-E_K)+|\Sigma_{cd}(z)|^2\mathcal{Z}_K]J_c(z)=0. \tag{9}$$

The logarithmic behavior of the self-energy part $J_c(z)$ means that it engenders single-particle resonances in the same region of the spectrum where a Kondo resonance exists. If the Fermi level lies sufficiently far from the band edge, so that $\mu-\varepsilon_c>T_K$, the Kondo resonance determines the tunneling current for $T<T_K$ in accordance with the results obtained in Ref. 4. However, for $\mu-\varepsilon_c<T_K$ the multiparticle resonance and the new edge resonances strongly influence one another. In this case the peak at the Fermi level can be mainly a potential resonance even for $T<T_K$. Writing the solution of Eq. (9) as $E_r=\epsilon_r+i\gamma_r$, we obtain that the low-energy poles of the T matrix are determined by the potential scattering under the condition

$$\frac{\gamma_r-T_K}{T_K}\gg\frac{\Lambda_{dc}}{(W_\nu\gamma_d)^{1/2}|\Lambda_{cc}|}\sim\left(\frac{\gamma_d}{W_\nu}\right)^{1/2} \tag{10}$$

(it was assumed that $\epsilon_r=\mu$). In this case we obtain from Eq. (9) the following expressions for the energies and widths of the potential resonance at the edge of the 2D band:

$$\epsilon_{r\pm}=\varepsilon_c\pm t_r\cos\,\alpha_r,\quad \gamma_{r\pm}=t_r\,\sin\,\alpha_r,\quad t_r=\gamma_0\,\exp\left(-\frac{1}{\Lambda'_{cc}}\right),\quad \alpha_r=\frac{4\Lambda''_{cc}}{(\Lambda'_{cc})^2}. \tag{11}$$

Here $\Lambda_{cc}=\tilde{\rho}_{0c}(\Sigma'_{cc}+i\Sigma''_{cc})$. A solution exists if $1/\Lambda'_{cc}>1$. For $\alpha_r\ll 1$ the resonance is split, and in the limit $\alpha_r\to\pi/2$ two resonances merge into one peak whose width is equal to t_r. Comparing the condition (10) with the conditions for the existence of an edge resonance, we can see that the condition (10) always holds as long as this resonance exists.

4. The tunneling transmittance is determined by the expression

$$\sigma(\mu)=2e^2\int dE\,\delta(E-\mu)\sum_{\mathbf{k}_\perp,\mathbf{k}'_\perp}W(\mathbf{k}_\perp,\mathbf{k}'_\perp;E).$$

We employ for the probability $W(\mathbf{k}_\perp,\mathbf{k}'_\perp;E)$ of elastic tunneling a Landauer-type formula, which represents the probability in terms of the $\mathcal{T}$ matrix: $\mathcal{T}=\hat{H}_t\hat{\mathcal{G}}\hat{H}_t$ (as shown in Ref. 10, the Landauer formula remains valid in the presence of Kondo scattering). We assume that the matrix element containing the Green's function $\mathcal{G}^{cc}$ makes the main contribution to the tunneling amplitude

$$\begin{aligned}W(\mathbf{k}_\perp,\mathbf{k}'_\perp,\varepsilon^L_{\mathbf{k}})&=|\mathcal{T}(\mathbf{k},\varepsilon^L_{\mathbf{k}};\mathbf{k}',\varepsilon^R_{\mathbf{k}'})|^2\delta(\varepsilon^L_{\mathbf{k}}-\varepsilon^R_{\mathbf{k}'})\\&=\sum_{\mathbf{p}_\perp,\mathbf{p}'_\perp}\Gamma^c_L(\mathbf{k}_\perp,\mathbf{p}_\perp;\varepsilon^L_{\mathbf{k}})\Gamma^c_R(\mathbf{k}'_\perp,\mathbf{p}'_\perp;\varepsilon^R_{\mathbf{k}'})\\&\quad\times\left|\frac{d\varepsilon_{\mathbf{k}'}}{dk'_l}\right||\mathcal{G}^{cc}_\sigma(\mathbf{p}_\perp,\mathbf{p}'_\perp;\varepsilon^L_{\mathbf{k}})|^2\delta(\varepsilon^L_{\mathbf{k}}-\varepsilon^R_{\mathbf{k}'}).\end{aligned} \tag{12}$$

The tunneling widths in this expression equal $\Gamma_\nu^c(\mathbf{k}_\perp,\mathbf{p}_\perp;\varepsilon_{\mathbf{k}}^\nu) = |T_c^\nu(\varepsilon_{\mathbf{k}}^\nu - \varepsilon_{\mathbf{p}_\perp}^\nu)|^2|B(\mathbf{k}_\perp)|^2|B(\mathbf{p}_\perp)|^2\rho_\nu(\varepsilon_{\mathbf{k}}^\nu - \varepsilon_{\mathbf{p}_\perp}^\nu)$. The tunneling transmittance contains regular and resonance contributions $\sigma(\mu)=\sigma_0(\mu)+\sigma_r(\mu)$. The regular contribution $\sigma_0(\mu)$ is due to tunneling via the 2D continuum:

$$\sigma_0(\mu)=\frac{e^2}{\pi}\frac{\Gamma_{0L}(\mu)\Gamma_{0R}(\mu)}{\Gamma_{0L}(\mu)+\Gamma_{0R}(\mu)}\rho_c(\mu), \quad \sum_\nu \Gamma_{0\nu}(\mu)=\sum_\nu |T_0^\nu(\mu)|^2\rho_\nu(\mu)\sim\gamma_0.$$

The sharp resonance peaks corresponding to the above-obtained new edge resonances will be seen against a background $\sigma_0(\mu)$ if $\gamma_0 \gg \max(\gamma_r,|\mu-\varepsilon_c|,t_r)$. Their contribution to the transmittance is determined by the expression

$$\sigma_r^m(\mu)=\frac{e^2}{\pi}F_r\frac{\Gamma_{0L}(\varepsilon_c)\Gamma_{0R}(\varepsilon_c)}{(\mu-\epsilon_m)^2+\gamma_m^2}[(\epsilon_m-\varepsilon_c)^2+\gamma_m^2]I^2(\mu), \quad F_r=\frac{4|\Sigma_{cc}|^2}{(\tilde{\rho}_{0c}\ \mathrm{Re}\ \Sigma_{cc})^2}, \tag{13}$$

$m=r^\pm$ for a split resonance and $m=r$ for an unsplit resonance,

$$I(\mu)=\sum_{\mathbf{k}_\perp}|B(\mathbf{k}_\perp)|^4|\mathcal{G}_{0\mathbf{k}_\perp}(\mu)|^2=\frac{1}{\pi}\tilde{\rho}_{0c}|B(\varepsilon_c)|^2\cdot\begin{cases}|\mu-\varepsilon_c|^{-1}, & \gamma_0\gg|\mu-\varepsilon_c|\gg\gamma_{r\pm}\\ \pi/2\gamma_r, & \gamma_0\gg\gamma_r\gg|\mu-\varepsilon_c|\end{cases} \tag{14}$$

for split and unsplit resonances, respectively. The maximum contribution to the transmittance with $\epsilon_m=\mu$ equals

$$\sigma_m^{\max}=\frac{\Gamma_{0L}\Gamma_{0R}}{(\Gamma_{0L}+\Gamma_{0R})^2}S_m, \quad S_m=F_m\left(\frac{\gamma_0}{\gamma_m}\right)^2\gg 1, \tag{15}$$

where $\gamma_m=t_r\alpha_r$, $\alpha_r\ll 1$, for a split resonance and $\gamma_m=t_r$ for an unsplit resonance. Therefore the resonance contribution to the transmittance has the form of either two peaks which are symmetric relative to the edge of the unperturbed two-dimensional band or one peak with $\mu=\varepsilon_c$. In both cases, as one can see from Eq. (15), we obtain an exponential increase in the transmittance in an elementary tunneling event as compared with the standard case of tunneling through a resonance impurity level.[3] This increase occurs for two reasons. First, the new resonances arise as a result of the potential scattering of ''evanescent'' states which exist in the region $\epsilon-\varepsilon_c<\gamma_0$ on electrons from the walls. For this reason, the widths of the obtained resonances are much smaller than the tunneling widths (in contrast to the standard shallow levels near the edge of the 2D band, which we studied in Ref. 7). Second, the transmittance contains an additional enhancement factor $I(\mu)$ associated with the proximity to the edge of the 2D continuum. On account of the last factor, the contribution of a single-particle resonance can be greater than the contribution of the Kondo resonance in the region $\mu-\varepsilon_c<T_K$ even when the condition (10) is satisfied. The ratio of the heights of the two peaks in the transmittance equals

$$\sigma_r^{\max}/\sigma_K^{\max}=W_\nu\gamma_d/\gamma_r^2. \tag{16}$$

We underscore that the new resonances exist in the regime of coherent tunneling between bands of different dimension in the energy range $\epsilon-\varepsilon_c<\gamma_0$. A remarkable feature of

these resonances is that they exist for any admissible position of a deep impurity level and, in contrast to a Kondo resonance at the Fermi level, they are temperature-independent.

This work was supported by the Russian Fund for Fundamental Research (Grants 96-02-18346 and 96-02-18235).

[1] L. Y. Chen and C. S. Ting, Phys. Rev. B **43**, 2097 (1991).
[2] N. S. Wingreen, K. W. Jacobsen, and J. W. Wilkins, Phys. Rev. B **40**, 11834 (1989).
[3] I. M. Lifshitz and V. Ya. Kirpichenkov, Zh. Éksp. Teor. Fiz. **77**, 989 (1979) [Sov. Phys. JETP **50**, 499 (1979)]; A. I. Larkin and K. A. Matveev, Zh. Éksp. Teor. Fiz. **93**, 1030 (1987) [Sov. Phys. JETP **66**, 580 (1987)]; L. I. Glazman and R. I. Shekhter, Zh. Éksp. Teor. Fiz. **94**, 292 (1988) [Sov. Phys. JETP **67**, 163 (1988)]; T. K. Ng and P. A. Lee, Phys. Rev. Lett. **61**, 1768 (1988).
[4] L. I. Glazman and M. E. Raikh, JETP Lett. **47**, 452 (1988); T. K. Ng, Phys. Rev. Lett. **70**, 3635 (1993); M. H. Hettler, J. Krona, and S. Hershfield, Phys. Rev. Lett. **73**, 1967 (1994).
[5] K. A. Matveev and A. I. Larkin, Phys. Rev. B **46**, 15337 (1992).
[6] L. I. Glazman and M. E. Raikh, JETP Lett. **48**, 445 (1988); Y. Meir, N. S. Wingreen, and P. A. Lee, Phys. Rev. Lett. **66**, 3048 (1991); D. C. Ralph and B. A. Burman, Phys. Rev. Lett. **72**, 3401 (1994).
[7] K. A. Kikoin and V. N. Fleurov, *Transition Metal Impurities in Semiconductors*, World Scientific, Singapore, 1994; K. A. Kikoin, L. A. Manakova, Fiz. Tekh. Poluprovodn. **29**, 291 (1995) [Sov. Phys. Semicond. **29**, 145 (1995)].
[8] A. C. Hewson, *The Kondo Problem to Heavy Fermions*, Cambridge University Press, Cambridge, 1993.
[9] C. Lacroix, J. Phys. F **11**, 2389 (1981).
[10] Y. Meir and N. S. Wingreen, Phys. Rev. Lett. **68**, 2512 (1992).

Translated by M. E. Alferieff

Fermionic entropy of the vortex state in *d*-wave superconductors

G. E. Volovik

Low Temperature Laboratory, Helsinki University of Technology, 02150 Espoo, Finland; L. D. Landau Institute of Theoretical Physics, 117940 Moscow, Russia; Centre de Recherches sur les Très Basses Températures, CNRS, 38042 Grenoble CEDEX 09, France

(Submitted 17 February 1997)
Pis'ma Zh. Éksp. Teor. Fiz. **65**, No. 6, 465–469 (25 March 1997)

In *d*-wave superconductors the electronic entropy associated with an isolated vortex diverges logarithmically with the size of the system even at low temperatures. In the vortex array the entropy per vortex per layer, S_V, is much larger than k_B and depends on the distribution of the velocity field v_s around the vortex. If there is a first-order transition upon a change of the velocity distribution, then there will be a big entropy jump $\Delta S_V \sim 1 k_B$ at the transition. This entropy jump comes from the electronic degrees of freedom on the vortex background, which is modified by the vortex transition. This can explain the big jump in the entropy observed in the so-called vortex-melting transition [A. Junod, M. Roulin, J-Y. Genoud *et al.*, Physica C, to be published], in which the vortex array and thus the velocity field are redistributed. The possibility of the Berezinskiı–Kosterlitz–Thouless transition in the 3-dimensional *d*-wave superconductor due to the fermionic bound states in the vortex background is discussed. © *1997 American Institute of Physics.* [S0021-3640(97)00606-3]

PACS numbers: 74.20.−z, 74.72.−h

1. GAP NODES AND SCALING

The low-energy properties of superconductors with nodes in the energy gap are governed by the electronic excitations close to the gap nodes. The electronic density of states (DOS) in the homogeneous superconductor is (see, e.g., the review[2])

$$N(E) \sim N_F \left(\frac{E}{T_c} \right)^{2-D}, \quad E \ll T_c, \tag{1}$$

where D is the dimension of the nodes and N_F is the DOS at the Fermi level in the normal metal. In the mixed state of superconductor the superflow around the vortex leads to a Doppler shift of the energy E to $E + \mathbf{v}_s(\mathbf{r}) \cdot \mathbf{p}$, where $\mathbf{v}_s(\mathbf{r})$ is the local superfluid velocity. This gives a finite DOS at zero energy:

$$N(0) \sim N_F \left(\frac{p_F v_s}{T_c} \right)^{2-D}. \tag{2}$$

Here v_s is the characteristic value of the superfluid velocity in the vortex array, given by $v_s \sim \hbar/m_3 R_V$, where $R_V \sim \xi(B_{c2}/B)^{1/2}$ is the intervortex distance, B is magnetic field, and $\xi \sim v_F/T_c$ is the coherence length. Thus $p_F v_s/T_c \sim \sqrt{B/B_{c2}}$, and this gives the following electronic DOS at zero energy as a function of magnetic field:

$$N(0) \sim N_F \left(\frac{B}{B_{c2}} \right)^{1-D/2}. \tag{3}$$

There are two different regimes, those of strong and weak fields, with the crossover parameter

$$x \sim \frac{T}{k_F v_s} \sim \frac{T}{T_c} \left(\frac{B_{c2}}{B} \right)^{1/2}, \tag{4}$$

which separates the superflow-dominated regime $x \ll 1$ from the temperature-dominated regime $x \gg 1$ (see Ref. 4). In general the thermodynamic functions depend on the parameter x. For example, the free energy of the excitations on the background of the vortex array is

$$F(T,B) = N_F T_c^2 \left(\frac{B}{B_{c2}} \right)^{2-D/2} \widetilde{F}(x), \tag{5}$$

where $\widetilde{F}(x)$ is the dimensionless function of the dimensionless parameter x. (See also the recent paper by Simon and Lee;[5] their crossover parameter differs from our by the factor $\sqrt{T_c/E_F}$. This is because Simon and Lee used the linearized spectrum of the fermions in the very vicinity of the gap nodes, which can be justified only at rather low temperature, $T \ll T_c^2/E_F$.) The normalization can be found from the low-field asymptote $x \gg 1$, where the largest contribution comes from the bulk superconductor, while the effect of vortices is small. It follows from Eq. (1) that the free energy of the homogeneous state $\sim -N_F T_c^2 (T/T_{c2})^{4-D}$, and this gives the following normalization of $F(T,B)$ and the low-field asymptote

$$\widetilde{F}(x) \sim -x^{4-D}, \quad x \gg 1. \tag{6}$$

2. SCALING FOR A *d*-WAVE SUPERCONDUCTOR

Free energy. In the case of nodal lines, i.e., for a node dimension $D=1$, one has the following estimate for the free energy of the excitations in the background of the vortex array:

$$F(T,B) = N_F T_c^2 \left(\frac{B}{B_{c2}} \right)^{3/2} \widetilde{F}(x). \tag{7}$$

Let us find the asymptotes of $\widetilde{F}(x)$ at $x \gg 1$ and $x \ll 1$. Let us consider first the weak-field case $x \gg 1$, i.e., the case of a dilute vortex array. In addition to the largest asymptote $\widetilde{F}(x) \sim -x^3$ from the bulk superconductor there is also the contribution from vortices. It comes from the modification of the normal-component density due to excitations: $\rho_n(T) \sim \rho N(T)/N_F$. This leads to a decrease of the kinetic energy of the superflow around the vortex, and thus the contribution to the energy of a vortex array with vortex density $n = B/\Phi_0$, where Φ_0 is the flux quantum, is

$$F(B\to 0)=-\frac{1}{2}n\rho_n(T)\int_{R_V>r>\hbar v_F/T} d^2r\ \mathbf{v}_s^2\sim -N_F T_c^2\frac{B}{B_{c2}}\frac{T}{T_c}\ \ln\frac{R_V T}{\xi T_c}. \tag{8}$$

This corresponds to the term $-x\ \ln x$ in $\widetilde{F}(x)$. So, the leading terms in the asymptote of $\widetilde{F}(x)$ at $x\gg 1$ are

$$\widetilde{F}(x)\sim -x\ \ln x - x^3, \quad x\gg 1. \tag{9}$$

The asymptote of $\widetilde{F}(x)$ at $x\ll 1$ is

$$\widetilde{F}(x)\sim -1-x^2, \quad x\ll 1. \tag{10}$$

Here both terms are from the vortices. The first one is temperature independent and does not contribute to the entropy or specific heat, but does contribute to the vortex magnetization. It comes from the nonzero normal-component density at $T=0$ due to the superfluid velocity: $\rho_n(T=0)\sim\rho N(E=0)/N_F\sim\rho(p_F v_s/T_c)^{2-D}$ (see Refs. 6–9):

$$F(T\to 0)=-\frac{1}{2}n\rho\int_{R_V>r>\xi} d^2r\ \mathbf{v}_s^2\left(\frac{p_F v_s}{T_c}\right)^{2-D}\sim -N_F T_c^2\left(\frac{B}{B_{c2}}\right)^{3/2}. \tag{11}$$

The second (quadratic in x) term in Eq. (10) gives a term linear in temperature to the specific heat: $C(T,B)\propto T\sqrt{B}$ (Ref. 3).

Vortex entropy. For the entropy density one has

$$S(T,B)=-\frac{\partial F}{\partial T}=N_F\frac{B}{B_{c2}}T_c\widetilde{S}(x), \tag{12}$$

$$\widetilde{S}(x)=-\frac{\partial\widetilde{F}}{\partial x}. \tag{13}$$

The asymptotes of $\widetilde{S}(x)$ at $x\gg 1$ and $x\ll 1$ are

$$\widetilde{S}(x)\sim\ln x+x^2, \quad x\gg 1, \tag{14}$$

$$\widetilde{S}(x)\sim x, \quad x\ll 1. \tag{15}$$

The vortex part of the normalized entropy $\widetilde{S}(x)$, i.e., without the bulk term x^2 in Eq. (14), can be written using the interpolating formula

$$\widetilde{S}(x)\sim\ln(x+1), \tag{16}$$

which gives both the logarithmic term in Eq. (14) at large x and the linear term in Eq. (15) at low x.

It is instructive to write the vortex entropy per vortex per layer

$$\frac{S_V(T,B)}{k_B}\sim\frac{E_F}{T_c}\ \ln(x+1), \tag{17}$$

where E_F is the Fermi energy. Note that the logarithmic vortex entropy in Eq. (14) also follows from the $1/E$ behavior of the vortex DOS found in Ref. 4. Using the result of Ref.

4, one can find an exact equation for the vortex entropy at large x using an axial distribution of the superfluid velocity around the vortex, $\mathbf{v}_s=(\hbar/2m_3r)\hat{\phi}$:

$$\frac{S_V(T,B)}{k_B}=2\ln 2\frac{v_F p_F}{\Delta'}\ln x, \quad x\gg 1. \tag{18}$$

Here Δ' is the angle derivative of the gap at the node.

Heat capacity. For the heat capacity one has

$$C(T,B)=T\frac{\partial S}{\partial T}=N_F T_c\frac{B}{B_{c2}}\widetilde{C}(x), \tag{19}$$

$$\widetilde{C}(x)=x\frac{\partial\widetilde{S}}{\partial x}. \tag{20}$$

Using the interpolating formula (17) for the entropy, one obtains interpolating formulas for the vortex part of the heat capacity

$$C(T,B)\sim N_F T_c\frac{B}{B_{c2}}\frac{x}{1+x}, \tag{21}$$

which gives both asymptotes found in Ref. 4: $\widetilde{C}(x)\sim x$ for $x\ll 1$ and $\widetilde{C}(x)\sim 1$ for $x\gg 1$.

3. DISCUSSION

The electronic entropy per vortex per layer, S_V in Eq. (17), is much larger than k_B even at $T\ll T_c$. For an isolated vortex this entropy diverges as the logarithm of the dimension R of the system: $S_V\sim k_B(E_F/T_c)\ln R$ (actually R is limited by the penetration length) and is at least a factor of $E_F/T_c\gg 1$ larger than the configurational entropy of the vortex in the 2-dimensional system, $S_{\rm conf}\sim k_B\ln R$. The logarithmic behavior of S_V, with R limited by the intervortex distance R_V, persists till $T\sim T_c\sqrt{B/B_{c2}}$ (or $x\sim 1$). Due to the large factor $E_F/T_c\gg 1$ the entropy per vortex per layer can be of order k_B even at $T<T_c\sqrt{B/B_{c2}}$ (or $x<1$), but it finally disappears in the high-field limit ($T\ll T_c\sqrt{B/B_{c2}}$ or $x\ll 1$).

It is important that S_V depends on the distribution of the velocity field $\mathbf{v}_s$ around the vortex. If there is a first-order transition upon a change in the velocity distribution, one can expect a big entropy jump, $\Delta S\sim 1k_B$. This entropy jump comes from the electronic degrees of freedom in the vortex background, which is modified by the vortex transition. This can explain the latent heat $L\sim 0.45k_BT$/vortex/layer observed on the so called vortex-melting line in a detwinned Y-123 crystal[10] and $L\sim 0.6\pm 0.1k_BT$/vortex/layer in a twinned sample of Y-123.[1] Even higher values of the entropy jump have been deduced from the magnetization measurements.[11] Such an entropy jump can occur both at the vortex-melting transition and at a first-order transition in which the structure of the vortex lattice changes, say, from a hexagonal lattice close to T_c to a distorted tetragonal lattice far from T_c. The latter structure was observed in Ref. 12 and is discussed in Ref. 13.

Note that the fermionic entropy of the 3-dimensional vortex loop of the length R is $\propto R \ln R$, as distinct from the configurational entropy of the loop $S_{\rm conf} \propto R$. This $R \ln R$ behavior of the vortex loop entropy, together with the large prefactor, can in principle cause a Berezinskiĭ–Kosterlitz–Thouless transition in the 3-dimensional system. This is supported by the following observation. It appears that if one uses the quantum-mechanical approach to the vortex DOS, by calculating the discrete bound states of the fermions on the background of the inhomogeneous distribution of the superflow around the vortex, one obtains a value of the vortex DOS that is twice as large as that obtained from a classical treatment of the fermions in terms of the Doppler shifted energy $E+\mathbf{v}_s(\mathbf{r})\cdot\mathbf{p}$ (Ref. 4).

The classical approach gives the conventional expression for the energy of isolated vortex in terms of the superfluid density $\rho_s(T)=\rho-\rho_n(T)$

$$F_V=\frac{\pi\hbar^2}{4m_e^2}(\rho-\rho_n(T))\ln\frac{R}{\xi}. \tag{22}$$

At low T, where $\rho_n(T)/\rho\sim T/T_c$, the second term corresponds to a logarithmic entropy of the vortex. The quantum-mechanical approach in terms of the fermionic bound states in the vortex background suggests the larger contribution of the fermions to the vortex entropy. This can be written using the enhancement factor $1+\alpha(T)$

$$F_V=\frac{\pi\hbar^2}{4m_e^2}[\rho-(1+\alpha(T))\rho_n(T)]\ln\frac{R}{\xi}. \tag{23}$$

According to Ref. 4 one has $\alpha(0)=1$. If this value of α persists to higher temperatures, the energy of an isolated vortex becomes zero at some temperature $T_V<T_c$, where $\rho_n(T_V)=\frac{1}{2}\rho$. Thus at T_V one would have the Berezinskiĭ–Kosterlitz–Thouless transition in the 3-dimensional system, occuring due to the essential contribution of the fermionic bound states to the vortex entropy. However, it is more natural to expect that $\alpha(T)$ decreases continuously with temperature, approaching zero at T_c, since the effect of the bound states should be negligible in the Ginzburg–Landau region. So, the possibility of the Berezinskiĭ–Kosterlitz–Thouless transition in this $3D$ system depends on the details of the behavior of $\alpha(T)$.

The author acknowledges the Centre de Recherches sur les tres Basses Temperatures (CNRS, Grenoble) and the Departement de Physique de la Matiere Condensee (Universite de Geneve) for hospitality and thanks O. Fischer, A. Junod, N. B. Kopnin, B. Revaz, and M. Dodgson for some stimulating discussions.

[1] A. Junod, M. Roulin, J-Y. Genoud *et al.*, Physica C, to be published.
[2] G. E. Volovik, cond-mat/9603094; Tr. J. Phys. **20**, 693 (1996).
[3] G. E. Volovik, JETP Lett. **58**, 469 (1993).
[4] N. B. Kopnin and G. E. Volovik, JETP Lett. **64**, 690 (1996).
[5] S. H. Simon and P. A. Lee, Phys. Rev. Lett. **78**, 1548 (1997).
[6] G. E. Volovik and V. P. Mineev, Zh. Éksp. Teor. Fiz. **81**, 989 (1981) [Sov. Phys. JETP **54**, 524 (1981)].
[7] P. Muzikar and D. Rainer, Phys. Rev. B **27**, 4243 (1983).
[8] K. Nagai, J. Low Temp. Phys. **55**, 233 (1984).
[9] D. Xu, S. Yip, and J. A. Sauls, Phys. Rev. B **51**, 16233 (1995).
[10] A. Schilling, R. A. Fisher, N. E. Phillips *et al.*, Nature **382**, 791 (1996).

[11] T. Nishizaki, Y. Onodera, T. Naito, and N. Kobayashi, J. Low Temp. Phys. **105**, 1183 (1996).
[12] I. Maggio-Aprile, Ch. Renner, A. Erb *et al.*, Phys. Rev. Lett. **75**, 2754 (1995).
[13] I. Affleck, M. Franz, and M. H. S. Amin, Phys. Rev. B **55**, R704 (1997).

Published in English in the original Russian journal. Edited by Steve Torstveit.

On the effect of a magnetic field on the yield point and kinetics of macroplasticity in LiF crystals

A. A. Urusovskaya, V. I. Al'shits, A. E. Smirnov, and N. N. Bekkauer
Institute of Crystallography,[a] *Russian Academy of Sciences, 117333 Moscow, Russia*

(Submitted 20 February 1997)
Pis'ma Zh. Éksp. Teor. Fiz. **65**, No. 6, 470–474 (25 March 1997)

A strong effect of a static magnetic field B on active deformation kinetics ($\dot{\epsilon}=$ const) in LiF crystals is observed. This is a threshold effect with respect to B and $\dot{\epsilon}$; it is observed only for $B>B_c$ ($B\simeq 0.4$ T) and $\dot{\epsilon}<\dot{\epsilon}_c$ ($\dot{\epsilon}_c\approx 10^{-4}$ s^{-1}). Magnetic sensitivity is exhibited by the yield stress τ_y, which decreases by approximately a factor of 1.5 for $B=0.48$ T, and by the stage-II and stage-III hardening coefficients $\theta_{\rm II}$ and $\theta_{\rm III}$, the former decreasing and the latter increasing in a magnetic field. A physical interpretation is proposed for the observed behavior.
 [S0021-3640(97)00706-8]

PACS numbers: 62.20.Fe, 75.90.+w

In 1987 it was discovered that individual dislocations in NaCl samples placed in a static magnetic field can move without the application of a mechanical load.[1] The basic properties of this new phenomenon, which has been termed the magnetoplastic effect, were studied in these and other nonmagnetic crystals in a subsequent series of intensive investigations by several independent groups.[2–14] First of all, it was established that the role of a magnetic field is to depin dislocations from paramagnetic obstacles. It is thought that this occurs as a result of spin evolution in a magnetic field, resulting in the removal of the spin-forbiddenness of the process, which radically changes the configuration of the system, destroying the barrier to dislocation motion. In this scheme, the depinning time $\tau_{\rm dp}$ of a dislocation is limited by the spin evolution in the system comprising the dislocation and paramagnetic center. It is obvious, however, that processes of this type can proceed only as long as appreciable spin–lattice relaxation does not occur over the time $\tau_{\rm dp}$. Otherwise, the thermal disordering of the spins should remove the effect. Taking into consideration the fact that the spin–lattice relaxation time τ_{sl} is virtually independent of the magnetic field and $\tau_{\rm dp}\propto B^{-2}$, it can be expected that there exists a threshold field B_c, determined by the estimate $\tau_{\rm dp}(B_c)\cong\tau_{sl}$, below which there should be no magnetoplasticity. Such a threshold has indeed been observed experimentally in a recent work.[13]

So far we have been talking about investigations of the effect of a magnetic field on microplasticity in crystals under conditions when the dislocation density ρ_d does not exceed values of the order of 10^4-10^5 cm^{-2}. At such densities ρ_d the dislocations pin one another relatively weakly. Indeed, in this case the average distance between ''forest'' dislocations that cross a slip plane is of the order of $1/\sqrt{\rho_d}\sim 100$ μm, and the average distance between impurity centers on a dislocation line in typical cases is no more than a

fraction of a micron. Therefore the ''switching off'' of point obstacles on dislocations in a magnetic field decreases the resistance to the motion of a dislocation by two to three orders of magnitude. This explains the experimentally observed motion of dislocations in a magnetic field under the influence of extremely low internal stresses (of the order of 0.01 MPa) as well as the high sensitivity of the dislocation mobility to weak external perturbations.[12]

At the same time, the question of greatest practical interest is the possibility of using the magnetoplastic effect to control the macroplasticity of nonmagnetic materials. This question is still open. It should be noted, however, that under conditions of macroplastic deformation the dislocation density ρ_d ordinarily is several orders of magnitude higher than the initial values and, correspondingly, the distance $1/\sqrt{\rho_d}$ is several orders of magnitude lower (for example, for $\rho_d \sim 10^8$ cm^{-2} we have $1/\sqrt{\rho_d} \sim 1$ μm). For this reason, such radical magnetic disordering of crystals as is observed in experiments with individual dislocations, unfortunately, cannot be expected in macroplasticity. However, in Ref. 9 an appreciable increase (by up to a factor of two) in the rate of strain $\dot{\epsilon}$ with increasing magnetic field was recorded in the hydraulic loading ($\dot{\sigma} =$ const) of a series of alkali-halide crystals in a magnetic field. Unfortunately, the authors could not measure by their method the effect of a magnetic field on such a fundamental characteristic as the yield stress τ_y.

From our standpoint the method of active deformation ($\dot{\epsilon} =$ const) is better suited for this purpose. This method makes it possible to measure multistage loading curves $\tau(\epsilon)$, which fix both τ_y and the hardening level at different stages of deformation. Our objective in the present work is to demonstrate observations of a strong magnetic effect on the kinetics of active deformation of LiF crystals, specifically, on the yield stress of these crystals.

The deformation experiments with and without a magnetic field were performed on a compression machine in which all parts located in the magnetic field region were made of nonmagnetic materials — aluminum, bronze, and brass. The compressing cross-heads (puncheons) consisted of ruby cylinders. The rate of strain varied from 10^{-5} to 10^{-3} s^{-1}. The temperature was equal to room temperature. The samples used were ''technically pure'' LiF crystals. Preliminary heat treatment of the samples was not performed. A magnetic field was produced by moving up a permanent magnet with an extensible pole separation. The magnetic induction could be varied from 0 to 0.5 T. Samples in the form of approximately $2.5 \times 2.5 \times 8$ mm parallelepipeds were cleaved along cleavage planes. The strain curves were automatically recorded on a KSP-4 recorder.

Three-stage strain curves were obtained during compression of LiF crystals with and without a magnetic field. The compression curves for two samples strained in the absence of magnetic field (curves *1* and *2*) and three samples compressed in a 0.48 T field (curves *3*, *4*, and *5*) are displayed in Fig. 1. Comparing the two series of curves shows that the slope of the initial rectilinear section, corresponding to elastic deformation of the crystals, is the same with and without a magnetic field. However, the yield stress τ_y in the case of tests in a magnetic field, just as the stresses τ_{II} and τ_{III} at the start of the deformation stages II and III, respectively, are much lower than in the case $B = 0$. One also notices a

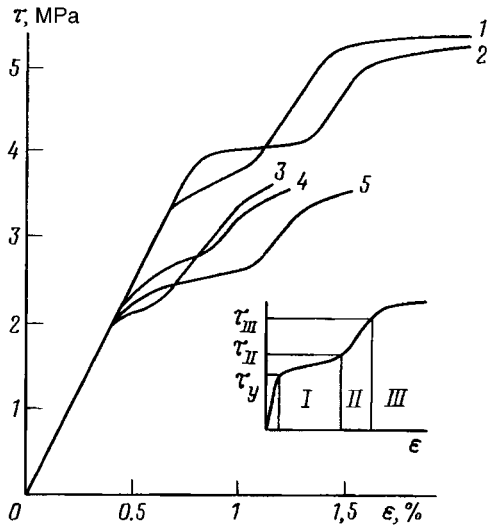

FIG. 1. Stress–strain curves for LiF crystals with no magnetic field (curves *1* and *2*) and in a 0.48 T field (curves *3*, *4*, and *5*); the rate of strain is $5\cdot 10^{-5}$ s^{-1}. Inset: Schematic stress–strain curve with the stages of deformation and the corresponding parameters indicated.

decrease in the slope of the curves $\tau(\epsilon)$ at the stage II of work hardening and an increase in the slope $\partial\tau/\partial\epsilon$ at the stage III of deformation in a magnetic field as compared with the corresponding slopes of the curves for $B=0$.

Figure 2 displays a series of curves of the above-noted characteristics as a function of the magnetic induction: the yield stress τ_y (a), the work-hardening coefficient $\theta_{\rm II}=(d\tau/d\epsilon)_{\rm II}$ (b), and the hardening coefficient at stage III of deformation $\theta_{\rm III}=(d\tau/d\epsilon)_{\rm III}$ (c). All curves pertain to a rate of strain $\dot{\epsilon}=5\cdot 10^{-5}$ s^{-1}. Similar dependences were also observed with a rate of strain of $\dot{\epsilon}=10^{-5}$ s^{-1}. However, at higher rates, starting at $\dot{\epsilon}=10^{-4}$ s^{-1}, the magnetic sensitivity of the curves $\tau(\epsilon)$ vanished.

The threshold character of the three magnetic field dependences in Fig. 2 correlates completely with the existence of the previously observed[13] threshold B_c of the magnetoplastic effect. Judging from Fig. 2, in the case at hand $B_c\approx 0.4$ T. The threshold with respect to $\dot{\epsilon}$ can also be qualitatively understood in the light of the model being developed here. A magnetic effect on the curves $\tau(\epsilon)$ should be observed only as long as the barrier-destroying spin-evolution time is shorter than the time required for a dislocation to overcome a barrier by thermal activation. Since the stress σ increases with the rate of strain $\dot{\epsilon}$, while the expectation time for thermal activation correspondingly decreases, it is clear that there should exist a threshold rate $\dot{\epsilon}_c$ above which the depinning of dislocations from point defects is limited by thermal fluctuation and not spin processes.

Investigation of strained samples in transmitted polarized light revealed that in fields $B>B_c$ only one pair of orthogonal slip planes (Fig. 3a) participates in deformation in a magnetic field, while without a magnetic field all four possible slip systems are always

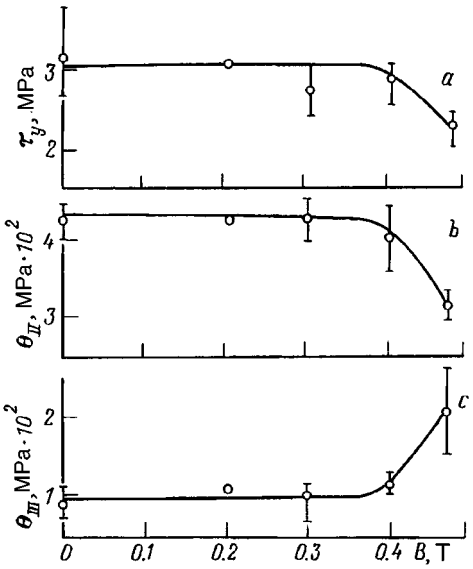

FIG. 2. Magnetic induction dependence of the yield stress τ_y (a), work-hardening coefficient θ_{II} (b), and stage-III hardening coefficient θ_{III} (c). The rate of strain is $5 \cdot 10^{-5}$ s^{-1}.

observed (Fig. 3b). It is important that in a magnetic field systems in which edge dislocations are parallel to the field become nonoperational. This is in complete agreement with the previously established fact that the magnetoplastic effect is not observed on edge dislocations oriented parallel to the field. At the same time, the decrease in the number of slip systems is naturally explained by the decrease in the work-hardening coefficient in a magnetic field (Fig. 2b).

It is well known that the transition to stage III of deformation occurs when the work performed by the dislocation sources is compensated by annihilation processes — mutual annihilation of dislocations of opposite mechanical signs. This decreases the hardening

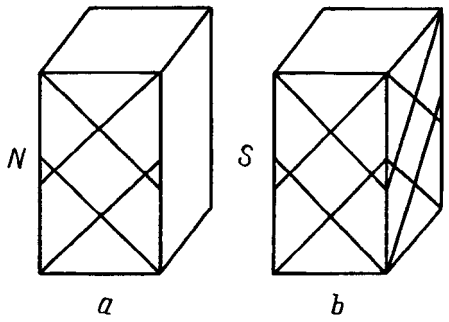

FIG. 3. Diagram of the arrangement of active slip systems in LiF crystals during deformation in a magnetic field (a) and without a field (b).

coefficient (the slope $\theta_{III}=(\partial\tau/\partial\epsilon)_{III}$ in stage III of deformation as compared with the corresponding level θ_{II} at stage II). Apparently, the same reserve of growth in the dislocation density which may be responsible for the increase in the slope θ_{III} for $B>B_c$ can also be provided by the slip systems which are not actuated at stage II during the straining of crystals in a magnetic field.

In summary, during the active deformation of LiF crystals there exists a quite appreciable macroscopic magnetoplastic effect in which the yield stress decreases substantially (by a factor of 1.5) at $B=0.48$ T. As the field increases further, the effect can be expected to become substantially stronger. In the light of the observed threshold nature of the effect with respect to B and $\dot{\epsilon}$, it is possible that in those cases where a pronounced effect of magnetic field on the plasticity of nonmagnetic materials is not observed (see, for example, Ref. 15), the reason could also be an unfortunate choice of experimental conditions (B and $\dot{\epsilon}$).

We are deeply grateful to A. L. Buchachenko, Yu. I. Golovin, and E. V. Darinskaya for helpful discussions.

[a)]e-mail: public@mechan.incr.msk.su

[1] V. I. Alshits, E. V. Darinskaya, T. M. Perekalina, and A. A. Urusovskaya, Fiz. Tverd. Tela (Leningrad) **29**, 467 (1987) [Sov. Phys. Solid State **29**, 265 (1987)].
[2] V. I. Alshits, E. V. Darinskaya, I. V. Gektina, and F. F. Lavrent'ev, Kristallografiya **34**, 1014 (1990) [Sov. Phys. Crystallogr. **34**, 597 (1990)].
[3] M. I. Molotskiĭ, Fiz. Tverd. Tela (Leningrad) **33**, 3112 (1991) [Sov. Phys. Solid State **33**, 1760 (1991)].
[4] V. I. Alshits, E. V. Darinskaya, and E. A. Petrzhik, Fiz. Tverd. Tela (Leningrad) **34**, 155 (1992) [Sov. Phys. Solid State **34**, 81 (1992)];V. I. Alshits, E. V. Darinskaya, and E. A. Petrzhik, Fiz. Tverd. Tela (St. Petersburg) **35**, 320 (1993) [Phys. Solid State **35**, 162 (1993)].
[5] M. I. Molotskiĭ, Fiz. Tverd. Tela (St. Petersburg) **35**, 11 (1993) [Phys. Solid State **35**, 5 (1993)].
[6] Yu. I. Golovin and R. B. Morgunov, Fiz. Tverd. Tela (St. Petersburg) **35**, 1384 (1993) [Phys. Solid State **35**, 700 (1993)].
[7] V. I. Alshits, T. V. Darinskaya, and T. A. Petrzhik, Mater. Sci. Eng. A **164**, 322 (1993).
[8] V. I. Alshits, E. V. Darinskaya, O. L. Kazakova, *et al.*, J. Alloys Compd. **211/212**, 548 (1994).
[9] Yu. I. Golovin and R. B. Morgunov, JETP Lett. **61**, 596 (1995).
[10] V. I. Alshits, E. V. Darinskaya, and O. L. Kazakova, JETP Lett. **62**, 375 (1995).
[11] M. I. Molotskii, R. E. Kris and V. Fleurov, Phys. Rev. B **51**, 12531 (1995).
[12] V. I. Alshits, E. V. Darinskaya, E. Yu. Mikhina, and E. A. Petrzhik, Fiz. Tverd. Tela (St. Petersburg) **38**, 2426 (1996) [Phys. Solid State **38**, 1333 (1996)].
[13] V. I. Alshits, E. V. Darinskaya, O. L. Kazakova *et al.*, JETP Lett. **63**, 668 (1996).
[14] Yu. I. Golovin and R. B. Morgunov, Fiz. Tverd. Tela (St. Petersburg) **37**, 1352 (1995) [Phys. Solid State **37**, 734 (1995)].
[15] D. N. Bol'shutkin, V. A. Desnenko, Fiz. Nizk. Temp. **7**, 652 (1981) [Sov. J. Low Temp. Phys. **7**, 321 (1981)].

Translated by M. E. Alferieff

Transport properties of $NdBa_2Cu_3O_{6+x}$ ceramics at the edge of the superconducting region upon a decrease in carrier density as a result of oxygen disordering in the $Cu–O_x$ planes

V. F. Gantmakher,[a] V. V. Sinitsyn, and G. É. Tsydynzhapov
Institute of Solid State Physics, Russian Academy of Sciences, 142432 Chernogolovka, Moscow Region, Russia

N. A. Doroshenko and V. P. D'yakonov[b]
Donetsk Physicotechnical Institute, Ukrainian National Academy of Sciences, 340114 Donetsk, Ukraine

(Submitted 21 February 1997)
Pis'ma Zh. Éksp. Teor. Fiz. **65**, No. 6, 475–480 (25 March 1997)

An initially nonsuperconducting ceramic sample with the composition $NdBa_2Cu_3O_{6+x}$ is brought, by means of pressure and quenching, to a state with a high carrier density and a superconducting transition, after which it is returned to the initial state by gradual annealing in several steps. The evolution of the magnetoresistance of the sample showed that even in the most resistive state realized in the experiment the superconducting interaction influences the resistance of the sample at fields all the way up to 5–6 T. In an 8 T field the change in resistance in this state in the temperature interval from 0.4 K to 20 K is described well by a logarithmic law $\Delta R \propto \log T$. © *1997 American Institute of Physics.* [S0021-3640(97)00806-2]

PACS numbers: 74.25.Fy, 74.72.Jt

The transport and superconducting properties of the compounds $RBa_2Cu_3O_{6+x}$ (R is a rare-earth element) are determined by the hole density n_h in the CuO_2 planes. Holes arise because electrons are transferred from these planes to the $Cu–O_x$ chain planes. Studies by many investigators have established that n_h depends not only on the oxygen concentration x in the $Cu–O_x$ planes but also on the arrangement of the oxygen in these planes, which can vary on account of the finite mobility of the oxygen atoms even at room temperature $T_r \approx 300$ K. The variants of the oxygen arrangement reduce to distributing oxygen over $Cu_{y+1}O_y$ chains of different length y.

It is well known that the density n_h and the superconducting transition temperature T_c decrease when the samples are heated to $T > T_r$ and then quenched in liquid nitrogen.[1,2] As the temperature increases, long $Cu_{y+1}O_y$ chains break up into shorter fragments, and the fraction of fragments with $y \leqslant 4$, which do practically no trapping of electrons from the CuO_2 planes and do not contribute to the formation of the carrier density n_h in them, increases.[3,4] When the quenched sample is held at room temperature T_r, the chains gradually increase in length, so that their average length $\overline{y}$ assumes an

equilibrium value $\overline{y(x,T_r)}$ within approximately one day. Accordingly, the density n_h also returns to its equilibrium value.

It is also possible to act on the oxygen subsystem by means of an external pressure P (see Ref. 5 and the references cited therein). The decrease in the volume of the unit cell in the compressed sample results in a higher equilibrium value $\overline{y(x,T,P)}$. Quenching can also preserve such a state of high density n_h after the pressure is removed. Annealing of such a sample at room temperature will decrease n_h and, correspondingly, T_c.

At values of x for which the sample is at the edge of the superconducting region (with densities n_h close to the critical values), a larger interval of n_h values can be spanned by applying pressure than by increasing the temperature. In Ref. 6 a transition temperature $T_c \approx 30$ K was achieved in an initially nonsuperconducting ceramic sample $NdBa_2Cu_3O_{6.67}$ by applying pressure, and then, with the pressure removed, the sample was returned to the initial state by holding at room temperature. We employed the effect of Ref. 6 to track the evolution of the temperature dependence of the resistance and magnetoresistance near the edge of the existence region of superconductivity in a single sample, i.e., on a fixed structural background.

We obtained the ceramic $NdBa_2Cu_3O_{6+x}$ by solid-phase synthesis of a mixture of neodymium and copper oxides and barium nitrate at temperatures of 900–1000 °C for a time of 8 h in an oxygen flow, grinding the intermediate product once. From the powder obtained, samples in the form of tablets 10 mm in diameter and 1.3 mm thick were pressed at a pressure of 0.7 GPa. Sintering was performed in an oxygen stream at $T=1000$ °C for 15 h, followed by cooling to 425 °C at a rate of 1 deg/min and holding periods of 3, 15, and 20 h at 650, 580, and 425 °C, respectively. The oxygen index x in the samples was determined by iodometric titration to be equal to 0.94. It was decreased nearly to the critical value by heating the samples in a nitrogen stream at 458 °C for 20 h and then cooling to room temperature (the value of x was calculated according to the change in weight). The critical value of x in the neodymium ceramic (R = Nd) is much higher than in the yttrium ceramic (R = Y).[7,8] In our sample the index x was equal to 0.67, just as in Ref. 6.

The dimensions of the sample were approximately $1\times2\times5$ mm. The resistance was measured by the standard four-contact method with the aid of pressure contacts consisting of pointed gold wires. The measurements were performed in a cryostat with pumping on He-3 vapor; a magnetic field of up to 8 T was produced with a superconducting solenoid.

The initial state of the ceramic, equilibrium at room temperature, was characterized by a rapid growth of the resistance with decreasing temperature, without any indications of a superconducting transition (Fig. 1, curve #1). Next, the sample was subjected to compression to a pressure of 1.5 GPa at room temperature for 24 h. The pressure treatment was conducted in a piston–cylinder type apparatus. Silicone was used as the pressure transmitting medium. To prevent the silicone from entering the pores in the ceramic, the sample was placed inside a rubber sheath which transmitted hydrostatic pressure well. The chamber was disassembled at room temperature, the process requiring 8 min, after which the sample was quenched in liquid nitrogen. The placement of the sample in the holder with the contacts was done at liquid nitrogen temperature without heating the

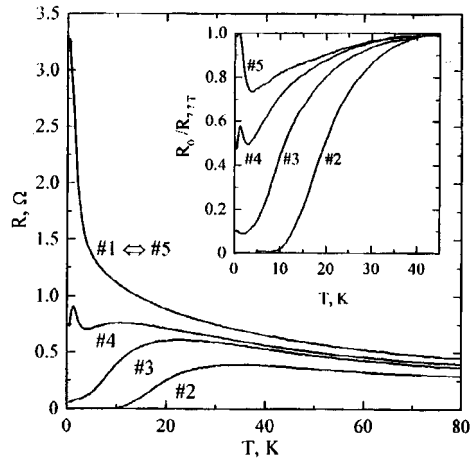

FIG. 1. Temperature dependences of the resistance of a $NdBa_2Cu_3O_{6.67}$ sample in zero magnetic field in states #1–#5 (states #1 and #5 are equivalent). Inset: Temperature dependences of the ratio of the resistances for all of these states in zero field and in a 7.7 T field.

sample. As a result, a sample with a complete superconducting transition starting at about 40 K and ending at 10 K was obtained (Fig. 1, curve #2). Next, the carrier density in the sample was decreased by heating the sample to room temperature; allowing the sample to stand for about 1 h substantially changed its state. In this manner, a series of different states was obtained (Fig. 1, curves #3 and #4). At the last stage the sample was held at room temperature for about two days. This gave the state #5, which, according to measurements of $R(T)$ and $R(H)$, was identical to the initial state, confirming that all changes are reversible.

In this manner, we obtained four states #2–#5 with different values of n_h and fundamentally different dependences $R(T)$. The magnetoresistance and its variation with temperature were measured for each state. The results are presented in the inset in Fig. 1 and in Figs. 2 and 3. We shall now proceed to a generalization and discussion of the results.

The superconducting response in granular materials has three components:[9]

a) London component — individual granules, becoming superconducting, shunt the resistance around themselves; this component is destroyed by the critical field $H_{c2}(T)$, which results in a positive derivative $\partial R/\partial H$;

b) Josephson component — a nondissipative current flows between neighboring superconducting granules and produces extended sections with no resistance; this state is destroyed by a field $H_J \ll H_{c2}$; and,

c) incoherent component — a single-particle current, which is less than the normal current because of the superconducting gap at the Fermi level, flows between a superconducting and a normal granule or between two superconducting granules but with the Josephson current suppressed; a field H, by destroying the gap, intensifies the single-particle current, which results in a negative derivative $\partial R/\partial H$.

These components all produce quite substantial changes in the resistance. For this

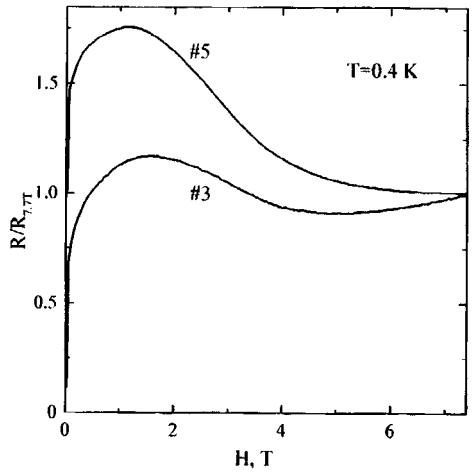

FIG. 2. Magnetic field dependences of the resistance in two different states (#3 and #5), $T=0.4$ K (compare with the temperature dependences $R(T)$ for the same states in Fig. 1).

reason, the very existence of a large magnetoresistance attests to the existence of a superconducting interaction, which is destroyed (or weakened) by a magnetic field, in a given state at a given temperature. For example, according to the inset in Fig. 1, the superconducting interaction in the state #2 first appears at 40 K and not 30 K, as one might conclude from the curve $R(T)$. In the most resistive state (#5) the $R(H)$ curve clearly exhibits manifestations of a superconducting interaction at $T=0.4$ K, while on the

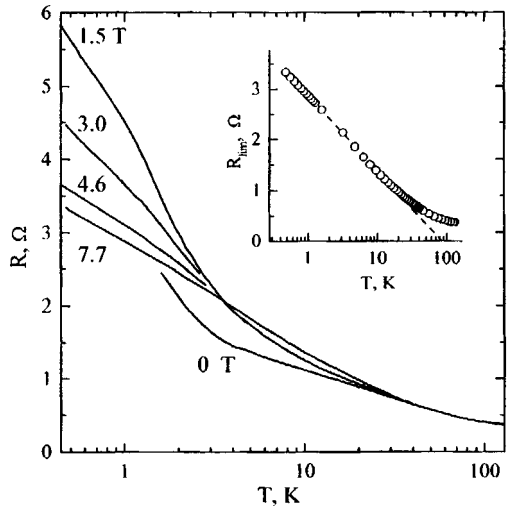

FIG. 3. Temperature dependences of the resistance in the state #5 in different magnetic fields. The limiting curve $R_{\rm lim}(\log T)$ (7.7 T field) is shown separately in the inset.

$R(T)$ curve these manifestations are masked by the increase in R with decreasing temperature.

All three components of the superconducting response can be distinguished in the curves $R(H)$ in Fig. 2. The rapid growth of the resistance in weak fields reflects the suppression of Josephson currents by a magnetic field; the region of negative slope $\partial R/\partial H$ reflects the growth of the single-particle current as a result of a decrease in the ratio Δ/T; and, finally, the positive derivative in strong fields for state #3 reflects the suppression of superconductivity in granules. The characteristic field H_{c2} is the same for the last two components, and the ratio between the components is determined by the temperature and structure of the sample: the average sizes and density of the superconducting granules as well as the transmittance of the contacts between them. It is known experimentally that the higher the normal-state resistance of the material, the larger the fraction of the incoherent component in the superconducting response.[9]

We now return to Fig. 3, where the curves $R(T)$ for the state #5 in different fields are presented. Even at our lowest temperature, 0.4 K, a 7.7 T field is already quite strong and the derivative $\partial R/\partial H$ in this field practically equals zero (see Fig. 2). We verified experimentally that $R(H)$ is saturated by 7.7 T at higher temperatures as well. This means that the curve $R(T)$ measured in a 7.7 T field is the limiting curve with respect to the family of such curves in weak fields: $R(T)_{7.7\,\mathrm{T}}=R_{\mathrm{lim}}(T)$. In the temperature range 4–30 K the family of curves approaches the limiting curve from below ($\partial R/\partial H>0$) and reaches the limiting values R_{lim} in fields of 1.5–2 T. For $T<4$ K the resistance R, increasing in weak fields, becomes much greater than R_{lim}, but the derivative $\partial R/\partial H$ changes sign in fields 1.5–2 T and becomes negative, so that the family approaches the limiting curve from above and reaches the curve in fields of 6–7 T.

In Fig. 3 the temperature is plotted on the abscissa in a logarithmic scale. In this scale the limiting curve $R(T)$ at $T<20$ K is a *straight line*. To underscore this basic experimental result of the present work, the curve $R_{\mathrm{lim}}(T)$ is once again plotted separately in the inset in Fig. 3. Such logarithmic temperature dependences have recently been observed in two other families of high-temperature superconductors — the systems $La_{2-x}Sr_xCuO_4$ (Refs. 10 and 11) and $Bi_2(Sr, La)_2CuO_{6+x}$ (Ref. 12). This is what motivated us to perform such an analysis of our results.

The physical mechanism leading to a logarithmic divergence in the low-temperature normal resistance of high-T_c superconductors is unclear at present. It should be noted that in the region of logarithmic temperature dependence the resistance varies by a factor of 4, i.e., the logarithmic term dominates. This signifies that weak-localization type processes cannot be responsible for the log T term. It is also difficult to invoke the Kondo effect to explain this dependence, since the curve $R_{\mathrm{lim}}(T)$ was measured in a quite strong field of 8 T, and similar curves were obtained in Refs. 10 and 11 even in a field of 60 T.

However, in this problem there are not only theoretical but also experimental ambiguities. Experiments must distinguish the dependence

$$\Delta R \propto \log T \tag{1}$$

from the dependences

$$1/R = a + bT^{1/n}, \quad n = 2 \text{ or } 3, \tag{2}$$

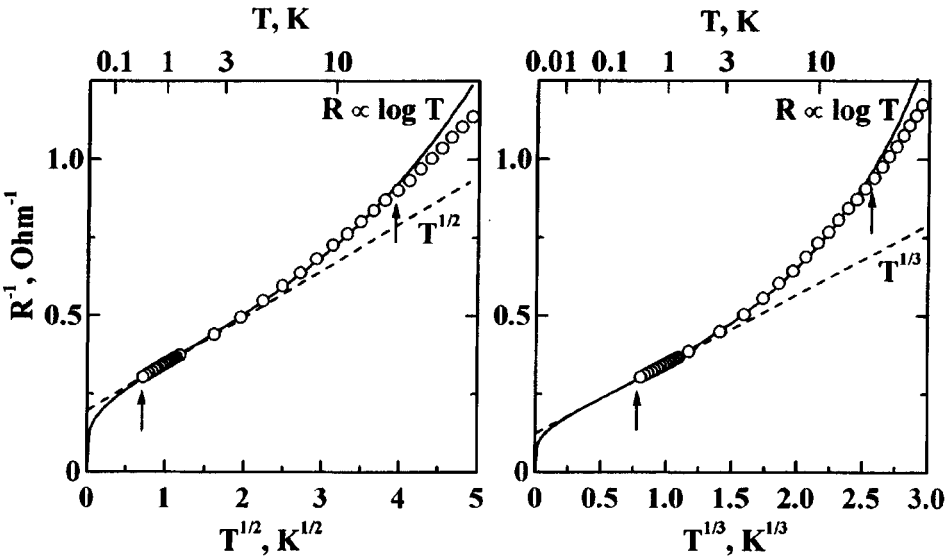

FIG. 4. Limiting values of the conductance $1/R_{\rm lim}$ as functions of $T^{1/2}$ and $T^{1/3}$. Solid line — description of the experimental data with the aid of log T. The arrows mark the temperature interval where this description agrees with experiment. The dashed straight lines demonstrate the region where the experimental data on $1/R_{\rm lim}$ can be described by a power-law function.

which follow from the scaling description of the neighborhood of the metal–insulator transition in a three-dimensional material[13] and have been repeatedly observed experimentally (see Ref. 14 and the references cited therein). Our results are presented in Fig. 4 in the scales $T^{1/2}$ and $T^{1/3}$. The temperature interval where the relation (2) describes the experimental data is narrower at the high-temperature end than in the case of relation (1). But at the low temperature end of the interval the differences in the descriptions (1) and (2) are smaller than the measurement accuracy, and it is obvious that even measurements performed on this sample at lower temperatures will not permit one to choose between these two descriptions. For this reason, experiments on other samples and materials must be performed in order to choose between the descriptions (1) and (2).

In summary, we have shown in experiments on the ceramic $NdBa_2Cu_3O_{6+x}$ that:

(a) The magnetoresistance (positive in weak fields and negative in strong fields) is much more sensitive to the presence of a superconducting interaction than is the function $R(T)$, and

(b) after superconductivity is destroyed by a magnetic field the temperature variations of the resistance below 20 K are described very well by the function log T.

We thank A. M. Lavrov for numerous discussions. This work was supported in part by the Russian Fund for Fundamental Research Grant 96-02-17497 and INTAS–RFBR Grant 95-302 and by the Government Program ''Statistical Physics.''

[a)]e-mail: gantm@issp.ac.ru
[b)]e-mail: dyakonov@host.dipt.donetsk.ua

[1] H. Claus, S. Yang, A. P. Paulicas *et al.*, Physica C **171**, 205 (1990).
[2] A. N. Lavrov and L. P. Kozeeva, Physica C **253**, 313 (1995).
[3] B. W. Veal and A. P. Paulicas, Physica C **184**, 321 (1991).
[4] G. V. Uimin, V. F. Gantmakher, A. M. Neminsky *et al.*, Physica C **192**, 481 (1992).
[5] W. H. Fietz, R. Quenzel, H. A. Ludwig *et al.*, Physica C **270**, 258 (1996).
[6] V. P. D'yakonov, I. M. Fita, N. A. Doroshenko *et al.*, JETP Lett. **63**, 825 (1996).
[7] H. Shaked, B. W. Veal, J. Faber Jr. *et al.*, Phys. Rev. B **41**, 4173 (1990).
[8] H. Lütgemeier, S. Schmenn, P. Meuffels *et al.*, Physica C **267**, 191 (1990).
[9] V. F. Gantmakher, V. N. Zverev, V. M. Teplinskiĭ, and O. I. Barkalov, Zh. Éksp. Teor. Fiz. **105**, 423 (1994) [JETP **78**, 226 (1994)].
[10] Y. Ando, G. S. Boebinger, A. Passner *et al.*, Phys. Rev. Lett. **75**, 4662 (1995).
[11] Y. Ando, G. S. Boebinger, A. Passner *et al.*, J. Low Temp. Phys. **105**, 867 (1996).
[12] R. Yoshizaki and H. Ikeda, Physica C **271**, 171 (1996).
[13] Y. Imry, J. Appl. Phys. **52**, 1817 (1981).
[14] V. F. Gantmakher, V. N. Zverev, V. M. Teplinskiĭ, and O. I. Barkalov, Zh. Éksp. Teor. Fiz. **103**, 1460 (1993) [JETP **76**, 714 (1993).

Translated by M. E. Alferieff

Field dependence of the anomalous Hall effect coefficient of granular alloys with giant magnetoresistance

A. B. Granovskiĭ, A. V. Kalitsov, and F. Brouers

M. V. Lomonosov Moscow State University, 119899 Moscow, Russia; Institut du Physique, Université de Liège, Sart Tilman, Liège 4000, Belgium

(Submitted 25 February 1997)
Pis'ma Zh. Éksp. Teor. Fiz. **65**, No. 6, 481–484 (25 March 1997)

It is shown theoretically that the anomalous Hall effect (AHE) coefficient R_s of magnetic granular alloys exhibiting giant magnetoresistance (GMR) depends strongly and, in the general case, nonmonotonically on the magnetic field as a result of the effect of the field on the character of the charge-carrier scattering and the AHE. The experimental data, presented by H. Sato, H. Hemmi, Y. Kobayashi *et al.*, J. Appl. Phys. **76**, 6919 (1994), on the field dependence $R_s(H)$ in Co–Ag granular alloys at low temperatures are explained. The presence of a maximum in the field dependence $|R_s(H)|$ in annealed Co–Ag alloys attests to the fact that skew scattering plays a dominant role in the formation of the AHE and that the main carriers of the AHE in these alloys are states whose spin polarization is directed oppositely to the magnetization. The presence of a minimum in this dependence for unannealed samples indicates nonuniformity of the granule size distribution. © *1997 American Institute of Physics.* [S0021-3640(97)00906-7]

PACS numbers: 73.40.Hm, 72.20.My, 75.70.Pa

The Hall field E_y in magnetic materials can be written in the form

$$E_y = R_0 B_z j_x + 4\pi R_s M_z j_x, \tag{1}$$

where B_z is the magnetic induction, M_z is the magnetization, j_x is the current density, R_0 is the normal Hall effect coefficient due to the action of the Lorentz force, and R_s is the anomalous Hall effect (AHE) coefficient. The AHE arises due to the effect of the spin-orbit interaction on the scattering of spin-polarized charge carriers.[1,2] The coefficient R_s is generally called the AHE constant, since for all previously investigated ferro-, antiferro-, and paramagnetic metals and alloys it does not depend on either the magnetization or the magnetic field.[1,2] However, it was recently discovered[3,4] that in systems exhibiting giant magnetoresistance (GMR) the AHE coefficient is a nonmonotonic function of the magnetic field, specifically, in granular alloys it exhibits a maximum or a minimum in fields of the order of 2–5 kOe. This letter proposes a simple explanation for this newly discovered behavior of the AHE and shows that both the dominant mechanism of the AHE and the main carriers of the AHE in specific granular alloys can be judged according to the form of the field dependence of R_s.

The essence of the proposed explanation is as follows. According to the definition (1)

$$R_s(H)=\frac{\sigma_{xy}(H)}{4\pi M_z}[\rho(H)]^2, \tag{2}$$

where σ_{xy} is the off-diagonal, linearly dependent on the spin-orbit interaction and therefore on M_z as well, part of the conductivity tensor and $\rho(H)$ is the total resistivity of the alloy in an external magnetic field H. The distinguishing feature of systems exhibiting GMR is that by changing the local magnetic configurations a magnetic field strongly influences the effective spin-dependent scattering potential V for spin-polarized charge carriers. For this reason, two factors determine the field dependence $R_s(H)$ — the substantial decrease in ρ when a field is applied and the effect of the magnetic field on σ_{xy}, the effect depending on both the polarization of the spins of the AHE carriers and on the specific scattering mechanisms. In the case of an asymmetric scattering mechanism (skew scattering), in the lowest approximation in the scattering potential V (Ref. 2)

$$\sigma_{xy}\sim\lambda\frac{\langle V^3\rangle}{\langle V^2\rangle^2}M_z, \tag{3}$$

where λ is the spin-orbit interaction constant and the brackets $\langle\ldots\rangle$ denote a configurational average. For this reason, the field dependences $R_s(H)$ and $(\rho(H))^2$ are different. In the case of the side-jump mechanism, as is well known,[2]

$$\sigma_{xy}\sim\lambda\frac{\langle V^4\rangle}{\langle V^2\rangle^2}M_z\sim\lambda M_z, \tag{4}$$

and therefore, according to expression (2), one should observe a correlation $R_s(H)\sim(\rho(H))^2$, which is not present in the experiment.[3,4] Hence it can be concluded that the skew scattering mechanism is the dominant AHE mechanism in granular alloys.

We shall now examine the possible types of field dependences of R_s accompanying skew scattering. Recently, we developed a method for calculating the AHE in granular alloys in the Zhang–Levy model.[5] This approach employs the concept of self-averaging of the scattering probability with electron scattering by a spin-dependent impurity potential in the volume of the granules, by the interface between granules and the matrix of the alloy, and in the volume of the matrix. This makes it possible to give a qualitative explanation of the GMR[6] and the AHE in sufficiently strong fields where $R_s\approx$ const.[5] Using this method, it is easy to obtain an expression for R_s in a granular alloy in an arbitrary magnetic field as well. Postulating that the field dependence of the magnetization $M(H)$ of a granular alloy is described by the Langevin function $L(H)$, we obtain for the contribution of carriers with spin in a direction opposite to the magnetization to the coefficient R_s

$$R_s^{\downarrow}(H)=\left[R_s^{b\downarrow}\frac{(1+p_b^2)^2}{(1+p_b)^4}\frac{(1-2p_bL(H)+p_b^2)}{(1-p_b)^2}+R_s^{s\downarrow}\frac{(1+p_s^2)^2}{(1+p_s)^4}\frac{(1-2p_sL(H)+p_s^2)}{(1-p_s)^2}\right]\frac{(\xi_0+\xi_1L(H))^2}{\xi_0^2}, \tag{5}$$

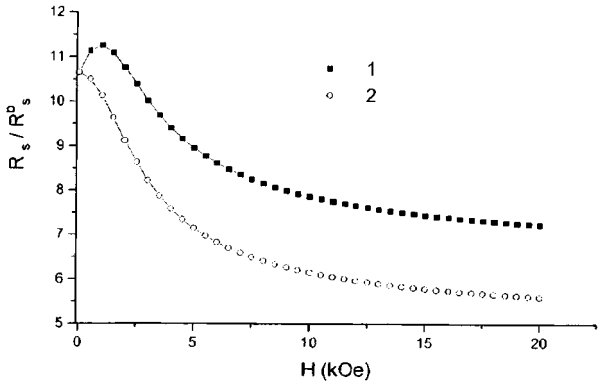

FIG. 1. Field dependence of the AHE coefficient R_s/R_s^b of annealed magnetic granular alloys ($c=0.2$, $p_b=0.2$, $p_s=0.52$, $l_m=50$ Å, $l_{nm}=250$ Å, $l_s/a_0=4$, $R_s^s/R_s^b=1$): $r_0=20$ Å (curve *1*), $r_0=80$ Å (curve *2*).

where

$$\xi_0=\frac{1-c}{l_{nm}}+\frac{c(1+p_b^2)}{l_m}+\frac{3c(1+p_s^2)}{r_0 l_s/a_0}, \tag{6}$$

$$\xi_1=\frac{2cp_b}{l_m}+\frac{6cp_s}{r_0 l_s/a_0}, \tag{7}$$

R_s^b and R_s^s are the values of the AHE coefficient in the volume and at the surface of the magnetic granules; l_{nm}, l_m, and l_s are, respectively, the average mean free path of conduction electrons in the matrix, granules, and on the surface of the granules; c is the volume density of granules; r_0 is the average radius of the granules; and, a_0 is the lattice constant. The parameters p_b and p_s characterize the ratio of the spin-dependent to the spin-independent impurity scattering potential in the volume and on the surface of the granules. For the contribution $R_s^{\uparrow}$ of carriers with spin in the direction of magnetization to R_s, in expression (5) p_b should be replaced by $-p_b$ and p_s should be replaced by $-p_s$.

The computational results obtained with Eqs. (5)–(7) for the field dependence of R_s in granular alloys, where the main AHE carriers are states with spin in a direction opposite to the magnetization (therefore $R_s^b<0$), are displayed in Fig. 1. The top curve was calculated with the parameters corresponding to real granular alloys with granule size $r_0\approx 20-80$ Å for which the amplitude of the GMR at low temperatures is $\approx 80\%$. In this case, a maximum is present in the field dependence $|R_s(H)|$; this agrees with the experimental data for annealed Co–Ag alloys (see Fig. 6 of Ref. 4). As the granule size increases, and correspondingly the role of surface scattering and GMR decreases, the extremum in $R_s(H)$ vanishes. Furthermore, for the contribution $R_s^{\uparrow}$ the extremum in the field dependence does not follow from the theory with arbitrary granule sizes. Hence it can be concluded that the main AHE carriers in the experimental Co–Ag

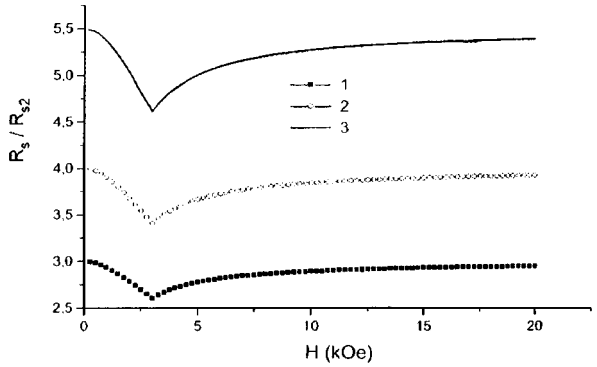

FIG. 2. Field dependence of the AHE coefficient R_s/R_s^b in unannealed magnetic granular alloys ($c_1=0.1$, $c_2=0.1$): $R_{s1}/R_{s2}=5$ (curve *1*), 7 (curve *2*), 10 (curve *3*).

granular alloys are states with spin in a direction opposite to the magnetization; this agrees with Kondorskiĭ's conclusion[7] about the types of main carriers AHE in 3*d* transition metals.

The expression (5) and the field dependences of R_s which are presented in Fig. 1 are valid only if the granules in the alloy all have approximately the same size, characteristic for the single-domain state. For unannealed granular alloys, both quite large ferromagnetic multidomain granules and single-domain particles can be dispersed in the nonmagnetic matrix. This can lead to a different type of field dependence $R_s(H)$ (see Fig. 2). For simplicity, let us assume that only two types of granules with concentrations c_1 and c_2 are present in the alloy, the AHE coefficients are R_{s1} and R_{s2}, and the electrical conductivity of the granules is the same as that of the matrix. Then, in the effective-medium theory[8] we obtain for the coefficient R_s of the alloy

$$R_s = c_1 R_{s1} \frac{M_1}{M} + c_2 R_{s2} \frac{M_2}{M}, \tag{8}$$

where $M=c_1M_1+c_2M_2$. For single-domain granules $M_1=M_0L(H)$, while for ferromagnetic granules we obtain $M_2(H)=M_0H/H_0$ for $H \leqslant H_0$ and $M_2=M_0$ for $H>H_0$. Then, as one can see from Fig. 2, the field dependence $|R_s(H)|$ is characterized by a minimum, in agreement with the experimental data for the AHE in unannealed Co–Ag samples.[4] The sharp kink in $R_s(H)$ at $H \approx H_0$ is evidently due to the crude model employed for the magnetization of large granules.

The following conclusions can be drawn on the basis of the foregoing analysis. The coefficient R_s in systems exhibiting GMR can depend on the field strongly, and even more strongly than does the resistance. The presence of a maximum in the dependence $|R_s(H)|$ in annealed Co–Ag alloys indicates that the skew scattering plays a dominant role in the formation in the AHE and also that the main AHE carriers in such alloys are states with spin in a direction opposite to the magnetic field. The presence of a minimum in the curve $|R_s(H)|$ for unannealed Co–Ag alloys attests to the fact that the granule size distribution in these alloys is nonuniform.

This work was supported by the Russian Fund for Fundamental Research (Grant 96-02-681a), INTAS (Grant 93-0718), and NATO (Grant HTECH.LG 951527).

[1] S. V. Vonsovskiĭ, *Magnetism* [in Russian], Nauka, Moscow, 1971.
[2] A. V. Vedyaev, A. B. Granovskiĭ, and O. A. Kotel'nikova, *Kinetic Phenomena in Disordered Ferromagnetic Alloys* [in Russian], Moscow State University Press, Moscow, 1992.
[3] H. Sato, Y. Kobayashi, Y. Aoki *et al.*, Phys. Rev. B **52**, 9823 (1995).
[4] H. Sato, H. Henmi, Y. Kobayashi *et al.*, J. Appl. Phys. **76**, 6919 (1994).
[5] A. Granovsky, F. Brouers, A. Kalitsov, and M. Chshiev, J. Magn. Magn. Mater. (to be published in 1997).
[6] S. Zhang and P. M. Lẹvy, J. Appl. Phys. **73**, 5315 (1993).
[7] E. I. Kondorskiĭ, Zh. Éksp. Teor. Fiz. **55**, 558 (1968) [Sov. Phys. JETP **28**, 291 (1968)].
[8] A. Granovsky, A. Vedyayev, and F. Brouers, J. Magn. Magn. Mater. **136**, 229 (1994)].

Translated by M. E. Alferieff